Article

Cell Reports

# Mutations of the AtYAK1 Kinase Suppress TOR Deficiency in *Arabidopsis*

## Graphical Abstract

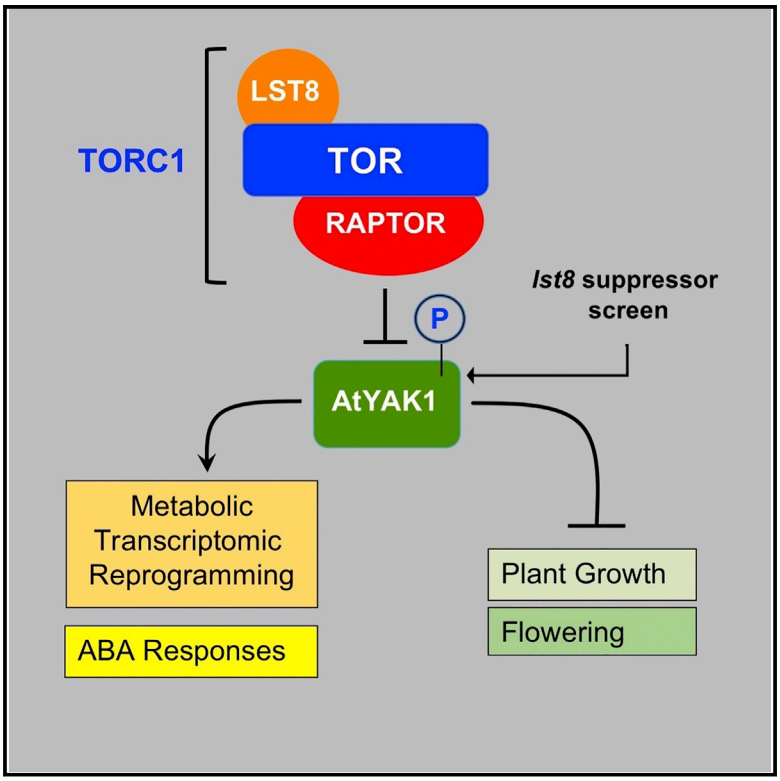


## Authors

Céline Forzani, Gustavo T. Duarte, Jelle Van Leene, ..., Geert De Jaeger, Anne-Sophie Leprince, Christian Meyer

## Correspondence

christian.meyer@inra.fr

## In Brief

The target of rapamycin (TOR) kinase is conserved in eukaryotes and controls growth and development. Forzani et al. find that mutations of the double-specificity plant YAK1 kinase restore growth of *lst8-1* mutants and dampen the effects of TOR deficiency. Moreover, they show that AtYAK1 is phosphorylated by TOR.

## Highlights

- A screen for suppressors of plant *lst8* mutants identifies the AtYAK1 kinase
- The AtYAK1 kinase interacts with RAPTOR and is phosphorylated by TOR
- *AtYAK1* disruption reduces transcriptional and metabolic changes in *lst8* mutants
- The ABA hypersensitivity of *lst8* mutants is reverted by *atyak1* mutations

Forzani et al., 2019, Cell Reports *27*, 3696–3708
June 18, 2019 
https://doi.org/10.1016/j.celrep.2019.05.074

CellPress

OPEN ACCESS
CellPress

Cell Reports
Article

# Mutations of the AtYAK1 Kinase Suppress TOR Deficiency in *Arabidopsis*

Céline Forzani,[1] Gustavo T. Duarte,[1] Jelle Van Leene,[2,3] Gilles Clément,[1] Stéphanie Huguet,[4,5] Christine Paysant-Le-Roux,[4,5] Raphaël Mercier,[1] Geert De Jaeger,[2,3] Anne-Sophie Leprince,[1,6] and Christian Meyer[1,7,*]

[1]Institut Jean-Pierre Bourgin, INRA, AgroParisTech, CNRS, Université Paris-Saclay, 78000 Versailles, France
[2]Department of Plant Biotechnology and Bioinformatics, Ghent University, Ghent, Belgium
[3]VIB Center for Plant Systems Biology, Ghent, Belgium
[4]Institute of Plant Sciences Paris-Saclay (IPS2), CNRS, INRA, Université Paris-Sud, Université d'Evry, Université Paris-Saclay, Bâtiment 630, Plateau de Moulon, 91192 Gif sur Yvette, France
[5]Institute of Plant Sciences Paris-Saclay (IPS2), CNRS, INRA, Université Paris-Diderot, Sorbonne Paris-Cité, Bâtiment 630, Plateau de Moulon, 91192 Gif sur Yvette, France
[6]Sorbonne Université, UFR 927, 4 Place Jussieu, F-75252 Paris Cedex 05, France
[7]Lead Contact
*Correspondence: christian.meyer@inra.fr
https://doi.org/10.1016/j.celrep.2019.05.074

## SUMMARY

**The target of rapamycin (TOR) kinase is a conserved energy sensor that regulates growth in response to environmental cues. However, little is known about the TOR signaling pathway in plants. We used *Arabidopsis* lines affected in the *lethal with SEC13 protein 8* (*LST8-1*) gene, a core element of the TOR complex, to search for suppressor mutations. Two suppressor lines with improved growth were isolated that carried mutations in the *Yet Another Kinase 1* (*AtYAK1*) gene encoding a member of the dual-specificity tyrosine phosphorylation-regulated kinase (DYRK) family. *Atyak1* mutations partly rescued the developmental defects of *lst8-1-1* mutants and conferred resistance to the TOR inhibitor AZD-8055. Moreover, *atyak1* mutations suppressed the transcriptomic and metabolic perturbations as well as the abscisic acid (ABA) hypersensitivity of the *lst8-1-1* mutants. AtYAK1 interacted with the regulatory-associated protein of TOR (RAPTOR), a component of the TOR complex, and was phosphorylated by TOR. Thus, our findings reveal that AtYAK1 is a TOR effector that probably needs to be switched off to activate plant growth.**

## INTRODUCTION

Recently the plant TOR (target of rapamycin) protein kinase has emerged as a central regulatory element transmitting external and internal information to control crucial cellular processes, including growth, mRNA translation, metabolism, and hormone- and pathogen-related responses (Rexin et al., 2015; Dobrenel et al., 2016a; Shi et al., 2018). The TOR protein kinase is a member of the phosphatidylinositol 3-kinase (PI3K)-related kinase (PIKK) family and is present throughout the eukaryotes. Its role was first described in yeast and animals, in which TOR is found in two protein complexes: TORC1 and TORC2 (Wullschleger et al., 2006; Albert and Hall, 2015; Blenis, 2017). Conversely, only the TORC1 complex has been described in photosynthetic organisms so far (Dobrenel et al., 2016a). TORC1 contains the TOR kinase and the core components regulatory-associated protein of TOR (RAPTOR) and lethal with SEC13 protein 8 (LST8).

The LST8 protein is a conserved and specific component of the TOR complex in eukaryotes (Díaz-Troya et al., 2008; Moreau et al., 2012; Baretić and Williams, 2014; Maegawa et al., 2015). The *LST8* gene was first identified in yeast by a screen for mutations showing synthetic lethality with mutations in *Sec13*, a gene involved in the transport of the nitrogen-regulated amino acid permease Gap1p to the plasma membrane (Roberg et al., 1997). The LST8 protein (called GβL in animals, for G protein β subunit like) contains seven WD 40 repeats, which are involved in the formation of a stable, propeller-like platform allowing interactions with several protein partners (Smith et al., 1999). Structure analyses indicate that LST8 interacts specifically with the TOR kinase domain. The binding site for LST8 is defined by a specific 40-amino-acid-long insertion in the TOR C lobe kinase domain, which is also conserved in plants. This domain is absent in other PI3K kinases, suggesting that the LST8-TOR interaction is specific. LST8 is necessary for TOR activation and is probably restricting access to the catalytical cleft (Yang et al., 2013; Aylett et al., 2016). It is likely that LST8 together with RAPTOR act as gatekeepers, controlling the recruitment and access of substrates to the TOR active site.

*Arabidopsis* possesses two copies of the *LST8* genes: *LST8-1* (At3g18140) and *LST8-2* (At2g22040). Only mutations in *LST8-1* result in retarded plant growth, increased branching, delayed flowering, reduced fertility, and hypersensitivity to a shift from short to long days (Moreau et al., 2012). The LST8-1 protein interacts with the TOR kinase domain and complements conditional *lst8* yeast mutants (Moreau et al., 2012). Moreover, *lst8-1* mutants have been found to be hypersensitive to the TOR inhibitor AZD-8055 and to abscisic acid (ABA) (Kravchenko et al., 2015).

 

Plant TOR is activated by nutrients or hormones like sugars and auxin, respectively, and promotes energy-consuming processes such as cell division, mRNA translation, and anabolism. On the other hand, TOR represses nutrient remobilization through autophagy during starvation or stresses (Dobrenel et al., 2016a; Baena-González and Hanson, 2017). In response to high sugar levels, TOR activates cell division in root and shoot meristems (Xiong et al., 2013; Pfeiffer et al., 2016). The TOR pathway also interacts with brassinosteroids during etiolated hypocotyl growth (Zhang et al., 2016) and inactivates ABA receptors by phosphorylation, thereby controlling plant responses to this stress-related hormone (Wang et al., 2018a).

A few TOR substrates have now been identified in plants, including the ribosomal protein S6 kinase (S6K) (Mahfouz et al., 2006), the type 2A phosphatase associated protein 46 kDa (TAP46) (Ahn et al., 2011), the PYL ABA receptors (Wang et al., 2018a), and the E2FA transcription factor (Xiong et al., 2013). Up to now, only two TOR regulators have been described in plants. The ROP2 GTPase activates TOR in response to auxin (Schepetilnikov et al., 2017; Li et al., 2017), and the conserved and antagonistic Snf1-related kinase 1 (SnRK1) inactivates the TOR complex by phosphorylating the RAPTOR protein (Nukarinen et al., 2016). However, a recent phosphoproteomic and interactomic analysis in *Arabidopsis* provided a large number of TOR targets (Van Leene et al., 2019). This study identified both known and unknown TOR substrates that contribute to different cellular processes and regulatory pathways with a significant number of TOR targets belonging to the translational machinery.

Aiming at identifying molecular components of the TOR signaling pathway, we undertook a genetic screen to isolate genetic modifiers of the *lst8-1-1* mutant. This mutant was selected since TOR functions in a complex together with LST8 and RAPTOR but only *lst8-1* or *raptor* mutants are viable. Therefore, by searching for *lst8* suppressors, we expected to identify molecular components of the TOR signaling pathway, which would function in growth control. We isolated two independent suppressor lines with nonsense mutations in Yet Another Kinase 1 (AtYAK1), which is a member of the dual-specificity tyrosine phosphorylation-regulated kinase (DYRK) family. The YAK1 kinase is also found in yeast with orthologs in animals, and functions in the regulation of growth and metabolism. Here, we show that loss-of-function mutations in the *AtYAK1* gene allow recovery of growth in *lst8-1-1* mutants by provoking reversion of both transcriptomic and metabolomic changes. The AtYAK1 protein interacted with RAPTOR and was phosphorylated *in vitro* by TOR. *Atyak1* mutations also resulted in a marked resistance to the TOR specific inhibitor AZD-8055 and suppressed the ABA hypersensitivity of the *lst8-1-1* mutants.

## RESULTS

### A Genetic Screen Identifies Mutations in *AtYAK1* That Suppress *lst8-1-1* Growth Defects

In order to understand TOR function, a suppressor screen was undertaken to isolate mutations suppressing the growth inhibition conferred by the absence of LST8, a TORC1 component. Seeds of the *lst8-1-1* transfer DNA (T-DNA) insertion mutant (Moreau et al., 2012) were mutagenized by ethyl methanesulfonate (EMS). Subsequently, the progenies of 1,500 M1 plants were screened for suppression of the *lst8-1-1* growth defect. The *lst8-1-1* mutant has a reduced growth rate and is sensitive to long days (LD) growth conditions (Moreau et al., 2012). M2 seeds were first screened *in vitro* for enhanced growth after 10 days in LD conditions. Plants showing faster growth were then transferred to soil for further screening in the greenhouse under the same day length. Six suppressor lines named suppressor of *lst8* (*sol*) were isolated (Figure S1A) based on their ability to grow and flower faster than the *lst8-1-1* mutant. However, none of the suppressor lines isolated were able to grow as well as the wild-type (WT) Col-0 control plants (Figures 1A and S1B). To identify the mutations responsible for this improved growth phenotype, the genome of the M2 suppressor lines and of the parental *lst8-1-1* mutant line was sequenced (see STAR Methods for details). Homozygous mutations present in the genome of the M2 suppressor lines were identified by using the MutDetect DNA pipeline analysis (Granier et al., 2016). Homozygous nucleotide base changes specific to the suppressor lines and absent from the parental *lst8-1-1* mutant were retained. Nucleotide changes resulting in nonsense mutations (stop codon, new or loss of start codon, mutations in splicing sites) were further analyzed. Two suppressor lines named *sol23* and *sol69* showed the strongest growth recovery. They were 15 and 14 nonsense mutations in the *sol23* and *sol69* lines, respectively (Data S1). The only gene in common was *AtYAK1* (At5g35980). In *sol23*, it contained a nonsense mutation (TGG $\geq$ TGA transition in the coding sequence producing the G924Stop mutation), and in *sol69* a splice-defect mutation at the end of the first intron affecting the acceptor site (transition G1438A, 1438 bp after the ATG of the AtYAK1 genomic sequence) was present (Figures 1B and S2A). An allelic test was performed by crossing these two *sol* lines, the results of which revealed that they are affected in the same gene (Figure S1C). The *atyak1* causal mutation in *sol23* was confirmed by genetic and cleaved amplified polymorphic sequence (CAPS) analysis of a segregating backcross F2 population of a cross between *sol23* and *lst8-1-1* (Figures S1D and S1E). In this F2 population, the *sol23* mutation segregated at a single locus and was recessive. AtYAK1 encodes a DYRK, and is the ortholog of the yeast YAK1 and animal DYRK1A kinases (Figures S2A and S2B). To further confirm that mutations in *AtYAK1* confer the suppressor phenotype in *sol23*, we used three loss-of-function alleles of *atyak1* (*atyak1-3*, *atyak1-4*, and *atyak1-5)* and tested whether they could suppress *lst8-1-1* as well as *lst8-1-2* (Moreau et al., 2012) mutant phenotypes by generating *lst8 atyak1* double-mutant combinations. The T-DNA insertion sites of the three *atyak1* alleles are shown in Figures 1B and S3A. The absence of the *AtYAK1* transcript in each line was confirmed by RT-PCR with primers spanning the T-DNA (Figure S3B). Each *atyak1* mutant allele, when introgressed in the *lst8-1-1* mutant background, was able to suppress the reduced shoot and root growth (Figures 1C–1F). Furthermore, the *lst8-1-2 atyak1-4* double mutant also showed an improved growth compared to *lst8-1-2*. The various *lst8 atyak1* double-mutant plants did not show equivalent growth to WT but their

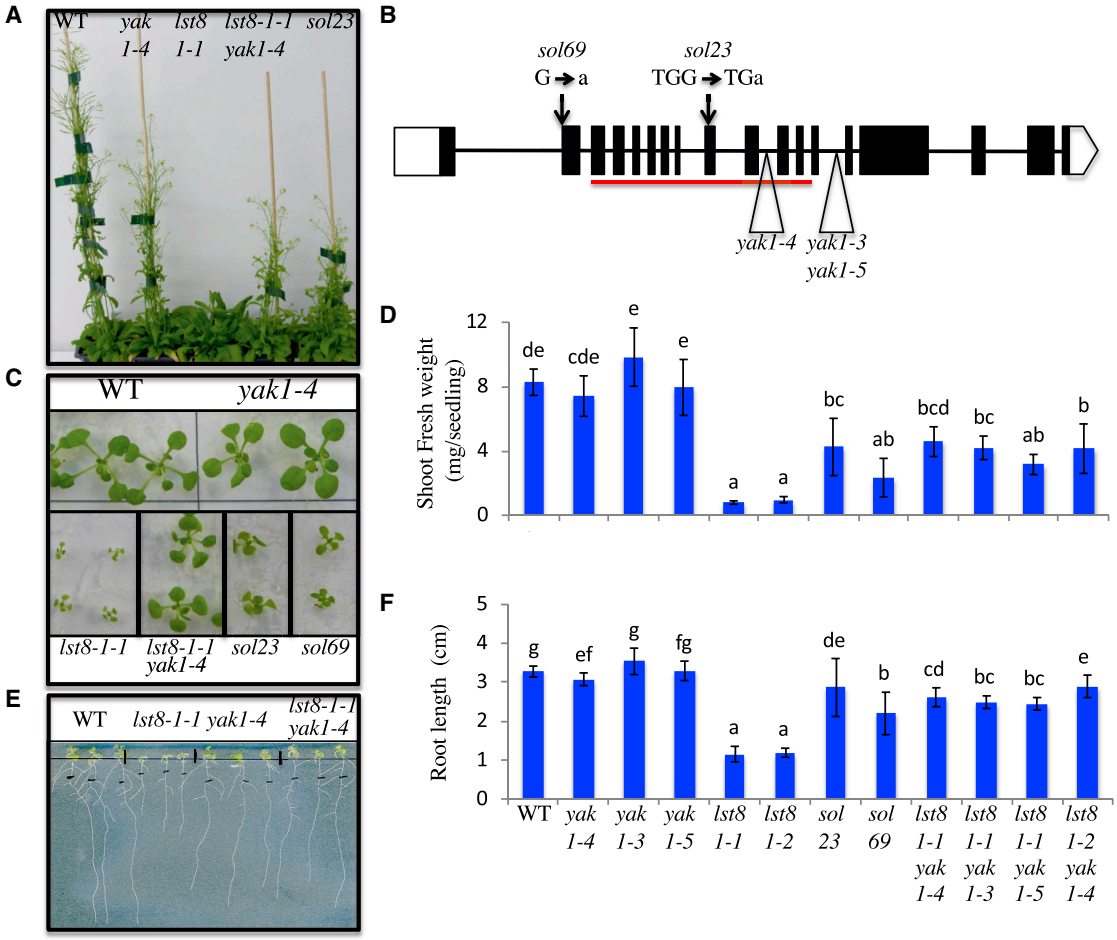


**Figure 1. *Atyak1* Mutations Suppress Growth Defects of *lst8-1* Mutant Plants**

(A) Fifty-day-old plants grown in soil under long-day (16 h of light, LD) conditions. A representative plant from each of the WT, *atyak1-4*, *lst8-1-1*, *lst8-1-1atyak1-4*, and *sol23* (suppressor of *lst8-1-1*) mutant lines is shown.

(B) Schematic representation of the *AtYAK1* gene (At5g35980) indicating the point mutations detected in *sol23* and *sol69* suppressor lines. The T-DNA insertion sites of the different *atyak1* mutant lines used in this study are depicted by triangles. Exons are shown in black boxes, black lines are the introns, and white boxes represent the 5′ or the 3′ untranslated regions. The red line indicates the putative kinase domain.

(C) Seedlings shown 14 days after transfer (DAT) and grown *in vitro*. Mutations in the *AtYAK1* gene restore growth to the *lst8-1-1 atyak1-4* double mutant.

(D) Quantification of the shoot fresh weight for the lines shown in (C) (14 DAT).

(E) The same lines were grown *in vitro* on vertical plates to determine root growth. Root growth shown 12 DAT.

(F) Quantification of the root length 7 DAT. Between 15 and 30 seedlings were measured for each genotype with three biological replicates. For (D) and (F), error bars indicate the standard deviation of three independent experiments. Letters indicate significantly different classes (non-parametric Kruskal-Wallis test, $p < 0.05$).

development was similar to *sol23* and *sol69*. Collectively, these findings indicate that the causal mutation in *sol23* and *sol69* is due to a mutation in *AtYAK1*.

### *Atyak1* Mutations Suppress the Delay in Flowering and Reduced Hypocotyl Growth Observed in *lst8-1* Mutants

Given the genetic burden of the suppressor lines that carry several mutations, we chose to continue our analysis using the *atyak1* T-DNA mutant alleles. We first tested whether *atyak1* mutations could reduce the flowering delay of *lst8-1-1* mutants. The *sol23* suppressor line and the *lst8-1-1 atyak1-4* double mutant flowered earlier than *lst8-1-1* but later than the WT or *atyak1-4* mutants (Figures 2A and S3C).

Next, we assessed whether LST8 was required for hypocotyl growth, because recent work by Huang et al. (2017) showed that *atyak1* mutants had longer hypocotyls compared to WT under low-light conditions. They proposed that AtYAK1 is a regulator of light responses since hypocotyl length can be used as a proxy for light perception and responses. Moreover, TOR was also shown to be necessary for hypocotyl elongation in the dark (Zhang et al., 2016). Therefore, we examined the hypocotyl of dark-grown mutants. The *lst8-1-1* mutants exhibited shorter hypocotyls compared to WT (Figure 2B). Again, *lst8-1-1 atyak1-4* double mutants showed increased hypocotyl growth compared to *lst8-1-1* but hypocotyl elongation was still decreased compared to the WT. These results further suggest

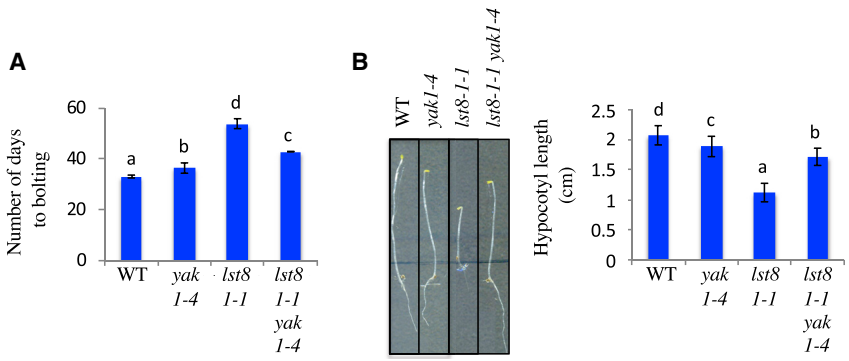


**Figure 2. The *Atyak1-4* Mutation Rescues *lst8-1-1* Growth Defects**

(A) Quantification of the flowering time by measuring the number of days to bolting. Plants were grown in LD conditions. Twelve plants were measured for each genotype. Two independent experiments were performed with similar results. Error bars indicate the standard deviation of a single experiment. Letters indicate significantly different classes (non-parametric Kruskal-Wallis test, $p < 0.05$).

(B) Seedlings grown *in vitro* in the dark on vertical plates for 6 days. The decrease in hypocotyl elongation observed in *lst8-1-1* mutants is suppressed by the *atyak1-4* mutant. Quantification of the hypocotyl length of 6-day-old dark-grown seedlings is shown. Between 10 and 30 seedlings were measured for each genotype with three biological repeats. Error bars indicate the standard deviation of three independent experiments. Letters indicate significantly different classes (non-parametric Kruskal-Wallis test, $p < 0.05$).

that the absence of AtYAK1 reduces the developmental defects and growth responses in the *lst8-1-1* mutant.

## AtYAK1 Acts in the TOR Signaling Pathway

We further analyzed whether the accelerated growth of *lst8-1-1 atyak1* mutants compared to *lst8-1-1* was due to altered TOR signaling. First, we measured the sensitivity to the specific TOR inhibitor AZD-8055 (Montané and Menand, 2013) of the different mutant lines. Figures 3A and 3B show that the three *atyak1* mutants are less sensitive to AZD-8055 compared to WT. *Atyak1* mutants have their root growth inhibited by 50% when transferred to *Arabidopsis* medium containing 1-μM AZD while WT roots are inhibited by 75%. In comparison to the WT, the two *lst8-1* mutants were more sensitive to AZD, while all the double-mutant *lst8-1 atyak1* combinations (Figure 3B) and *sol23* (Figure S3D) were less sensitive to AZD-8055. *Atyak1* mutants and *lst8-1 atyak1* double mutants showed a similar AZD-8055 root growth inhibition.

We then investigated whether an increase in TOR activity could be detected in the *atyak1* mutants in order to explain the AZD-8055-resistant phenotype. We have previously developed a new assay to measure TOR activity (Dobrenel et al., 2016b) that is based on the indirect TOR phosphorylation of the ribosomal protein S6 (RPS6) through activation of the S6 kinase. By using a phospho-specific antibody recognizing the phosphorylated Ser240 in RPS6, a correlation between the level of RPS6 phosphorylation and TOR activity was previously shown by western blot analysis (Dobrenel et al., 2016b). Therefore, just as for animals and yeast, RPS6 phosphorylation can be used as a readout for TOR activity in *Arabidopsis*. By using this assay, we showed that the sucrose-promoted TOR activity is reduced in the *lst8-1-1* or *lst8-1-2* mutant plants compared to WT (Figure 3C). However, no changes in TOR activity were observed in the three *atyak1* alleles compared to WT. Furthermore, the induction of TOR activity was not restored in the *lst8-1 atyak1* double mutants or *sol23* (Figure S3E), suggesting that AtYAK1 could be a downstream TOR effector.

## AtYAK1 Interacts with RAPTOR1B and Is a Substrate of TOR

Given that LST8 as well as RAPTOR are required to maintain the stability of the TORC1 complex and to recruit regulators or substrates of TOR, we tested whether LST8-1 or RAPTOR1B (At3g08850) could directly interact with AtYAK1. The interaction between these different proteins was evaluated by a yeast two-hybrid assay using a *HIS3* reporter gene. Only when yeast cells were expressing RAPTOR1B fused to the GAL4 DNA binding domain (BD-RPT) and AtYAK1 fused to the GAL4 activation domain (AD-YAK) were they able to grow on a selective media lacking histidine (Figure 4A). Therefore, RAPTOR1B physically interacts with AtYAK1, possibly for recruiting it to the TORC1 complex.

The interaction between AtYAK1 and RAPTOR1B was confirmed in plant cells by using bimolecular fluorescence complementation (BiFC) assays. *AtYAK1*, *RAPTOR1B*, and *LST8* genes were fused in frame to the N- or C-terminal half of YFP. Different combinations of vectors were then transiently expressed in *Nicotiana benthamiana* epidermal leaf cells. As shown in Figure 4B a fluorescent signal was observed for AtYAK1 and RAPTOR1B at the periphery of the cells. No interaction was detected between AtYAK1 and LST8 or between RAPTOR1B and LST8 proteins. These results demonstrate a specific interaction between AtYAK1 and RAPTOR1B *in vivo*.

Since AtYAK1 interacts with RAPTOR1B, we determined whether *Arabidopsis* TOR is able to phosphorylate the AtYAK1 protein. Using the phosphoproteomic analysis performed by Van Leene et al. (2019) in cell cultures in response to TOR inhibition, we extracted the data showing that AtYAK1 is phosphorylated on Ser505 and Ser847. This phosphorylation is inhibited by the TOR inhibitor AZD-8055 (Figure S4), suggesting that AtYAK1 is a TOR target. These phosphorylated sites are found in plant YAK1 (Figure S2A), but seem to be absent in animal DYRK1A sequences, while yeast YAK1 is lacking the C-terminal domain containing the phosphorylated Ser847.

To further validate that TOR phosphorylates AtYAK1, we performed *in vitro* kinase assays. AtYAK1 was purified as a recombinant His-MBP-AtYAK1 protein in *E. coli* but was capable of strong autophosphorylation activity (Figure 4C). AtYAK1 has been previously shown to autophosphorylate on serine (Ser) and tyrosine (Tyr) residues (Kline et al., 2010; Kim et al., 2015). We then used INDY, a specific inhibitor of the animal AtYAK1 homolog DYRK1A kinase (Ogawa et al., 2010), to inhibit AtYAK1 activity that would otherwise obscure TOR kinase activity. INDY

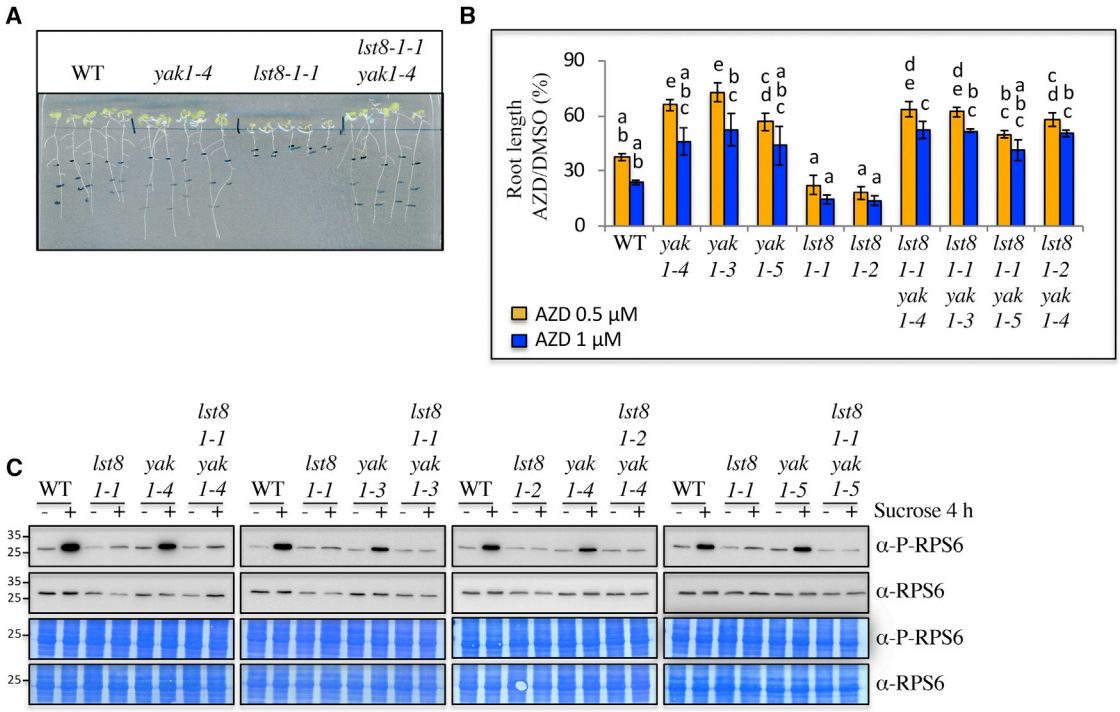


**Figure 3. AtYAK1 Is Part of the TOR Signaling Cascade**

(A) Eleven-day-old seedlings grown on *Arabidopsis* medium supplemented with 1 μM of the TOR-specific inhibitor AZD-8055. The hypersensitivity to AZD-8055 observed in *lst8-1* mutants is suppressed by *atyak1* mutations.

(B) Quantification of the root length 7 DAT on *Arabidopsis* medium supplemented with 0.5 or 1 μM of AZD-8055. Between 15 and 30 seedlings were measured for each genotype with three biological replicates. Error bars indicate the standard deviation of three independent experiments. Letters indicate significantly different classes (non-parametric Kruskal-Wallis test, $p < 0.05$).

(C) Determination of TOR activity using phosphorylation of the ribosomal protein S6 as a readout. Total protein extracts from seedlings were used for immunoblotting with a phospho-specific antibody against phosphorylated RPS6 (α-P-RPS6) or an antibody recognizing total RPS6 (α-RPS6). Bottom panels show the Coomassie Brilliant Blue staining of the membrane. Six-day-old seedlings from WT, *lst8* (two mutant alleles), *atyak1* (three mutant alleles), and *lst8 atyak1* double-mutant combinations were transferred to sugar-free medium for 24 h and then either mock (−) or 0.5% sucrose (+) treated for 4 h.

significantly reduced the autophosphorylation of recombinant AtYAK1 protein (Figure 4C). Next, we examined if tandem-affinity-purified (TAP) TOR complexes, obtained from *Arabidopsis* cell cultures using the $GS^{rhino}$-RAPTOR1B fusion protein as bait (Van Leene et al., 2019), were able to phosphorylate the recombinant AtYAK1 protein *in vitro*. To correct for phosphorylation by potential contaminating kinases, negative controls were performed in which an equal amount of substrate was incubated with non-specific proteins purified through TAP on WT cell cultures (Figure 4C; TAP WT control), as reported previously (Van Leene et al., 2019). Moreover, because the tagged RAPTOR1B protein (153 kDa) is phosphorylated during the *in vitro* kinase assay by the TOR kinase, showing a phosphorylation band that migrates at approximately the size of the recombinant His-MBP-AtYAK1 fusion protein (147 kDa), we removed the streptavidin beads bearing the tagged $GS^{rhino}$-RAPTOR1B protein after the kinase assay by centrifugation through a filter (Figure 4C, minus TAP beads). When INDY-inhibited AtYAK1 recombinant protein was combined with the TOR fraction, phosphorylation of the AtYAK1 fusion protein was observed (Figure 4C). Taken together, we conclude that AtYAK1 is very likely a TOR substrate since AtYAK1 is phosphorylated *in vitro* by TOR, *in planta* in a TOR-dependent manner, and is interacting with RAPTOR.

## The Metabolic Changes Observed in *lst8-1-1* Are Partly Mediated by AtYAK1

In previous studies, *lst8-1-1* mutant plants were shown to have altered metabolic responses with elevated amino acid levels (Moreau et al., 2012). A global metabolic profile analysis was therefore performed to determine if the *atyak1-4* mutation is able to suppress the metabolic changes observed in *lst8-1-1*. The metabolites were extracted from 7-day-old seedlings of WT, *atyak1-4*, *lst8-1-1*, and *lst8-1-1 atyak1-4* mutants and were analyzed by gas chromatography-mass spectrometry (GC-MS). The hierarchical cluster analysis showed a global reversion of metabolite levels in *lst8-1-1 atyak1-4* double mutants compared to *lst8-1-1* (Figure S5; see Data S2 for raw data). In particular, the amino acid increase occurring in *lst8-1-1* mutants is reduced in *lst8-1-1 atyak1-4* double mutants (Figure 5A). Among the 19 amino acids that showed increased levels in *lst8-1-1*, 15 accumulated to a lesser extent in the *lst8-1-1 atyak1-4* double mutant, with the exception of aspartate, glutamate, phenylalanine, and proline, for which the variations were not statistically significant

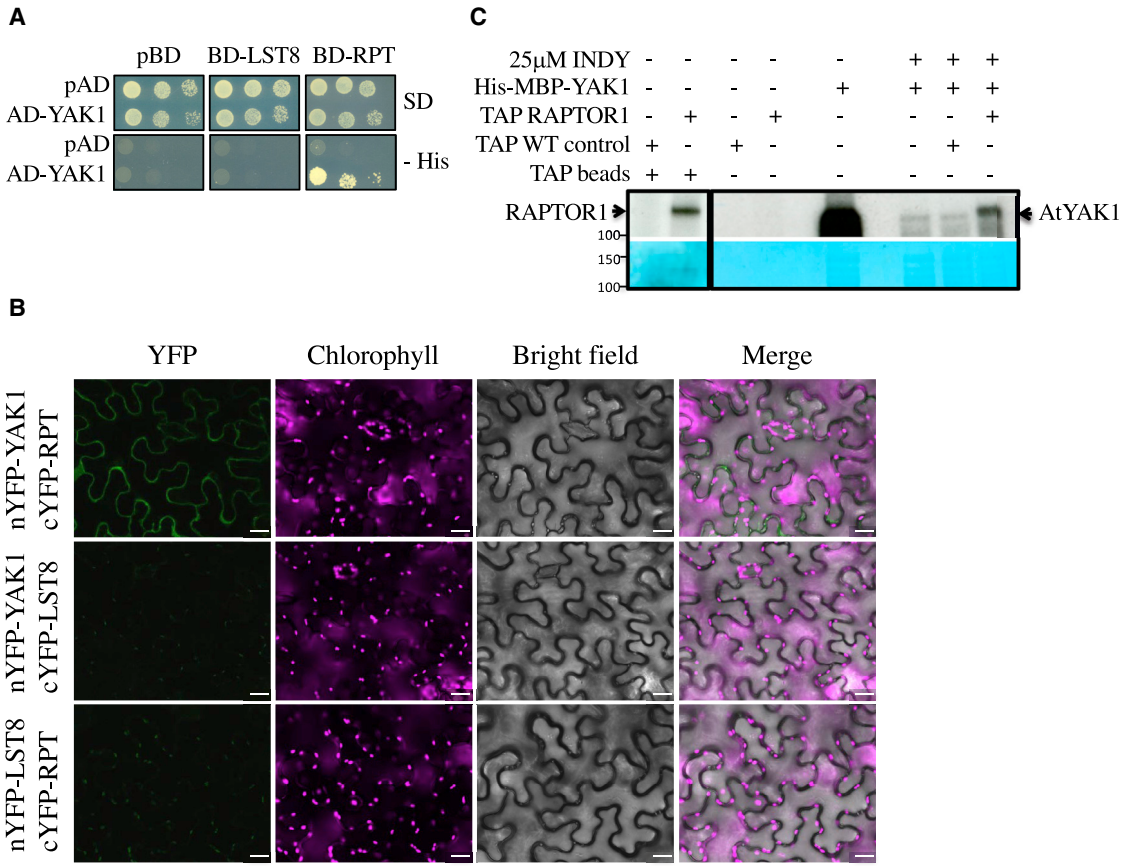


**Figure 4. AtYAK1 Interacts with RAPTOR1B in Yeast and Plant Cells and Is Phosphorylated by TOR Fractions *In Vitro***

(A) Yeast two-hybrid assays with LST8 (BD-LST8) or RAPTOR (BD-RPT) fused to the GAL4 DNA binding domain or the empty vector pBD, with AtYAK1 (AD-YAK1) fused to the GAL4 activation domain or empty vector pAD. Ten-fold serial dilutions were spotted onto SD agar medium control plates (SD) or plates lacking histidine containing 0.4-mM 3-Amino-1,2,3-triazole (-His).

(B) Bimolecular fluorescence (BiFC) experiments in *Nicotiana benthamiana*. Confocal images of *N. benthamiana* epidermal cells co-infiltrated with N-terminal or C-terminal YFP moieties fused to the proteins of interest (nYFP and cYFP, repectively). The vector pairs are indicated on the left. From right to left: YFP, chlorophyll from chloroplast autofluorescence, bright field, and merge panels. Scale bars, 20 μm.

(C) The TOR complex was purified by tandem-affinity purification (TAP) from *Arabidopsis* cell cultures expressing a N-GS$^{rhino}$-Raptor1B fusion protein (TAP Raptor1B). As a negative control, TAPs were performed on WT cell cultures (TAP WT control). AtYAK1 was fused to the His-MBP tag and produced from *E. coli*. AtYAK1 autophosphorylation activity was inhibited by 25 μM INDY, a specific DYRK1A inhibitor. RAPTOR1B-coated TAP beads were removed (–) or not (+) by centrifugation after the kinase assay. The top panel shows the kinase assay visualized by autoradiography and the bottom panel shows the Coomassie Brilliant Blue staining of substrates as loading control.

(Figure 5A). The most striking increase was measured for glutamine, which was 134-fold more abundant in *lst8-1-1* compared to WT (Figure 5B). Amino acids such as arginine are also the precursors for the synthesis of polyamines and components of this pathway such as agmatine and putrescine accumulated in *lst8-1-1* but not in *lst8-1-1 atyak1-4.*

Compared to this strong amino acid response, changes in sugars such as mannose, galactose, and arabinose, or in the levels of tricarboxylic acid (TCA) cycle intermediates such as malate, were less important. Again, the levels of these metabolites were reduced in *lst8-1-1 atyak1-4* double mutants compared to *lst8-1-1,* apart from sucrose. No significant changes to WT were measured for fructose and glucose in *lst8-1-1*. Altogether, this output indicates that AtYAK1 activity could be mediating part of the metabolic changes occurring in *lst8-1-1* mutants.

## Mutations in *AtYAK1* Partly Reduce the Gene Expression Changes Observed in *lst8-1-1* Mutants

To gain further insight into the molecular processes involved in the suppression of the *lst8-1-1* growth phenotype by the *atyak1* mutation, we used RNA sequencing (RNA-seq) to explore transcriptome variations. Seedlings of Col-0 WT, *lst8-1-1*, *atyak1-4*, and *lst8-1-1 atyak1-4* double mutants were grown *in vitro* for 7 days. RNA was extracted from three biological replicates and sequenced. The reads were mapped to the *Arabidopsis* Tair10 genome version. Expression levels were compared for each gene between the samples, and only the genes for which the variations were significantly different were retained for further analysis (p value < 0.05; see STAR Methods for details).

As observed previously (Moreau et al., 2012), mutations in the *LST8* gene resulted in large changes of the transcriptome profile

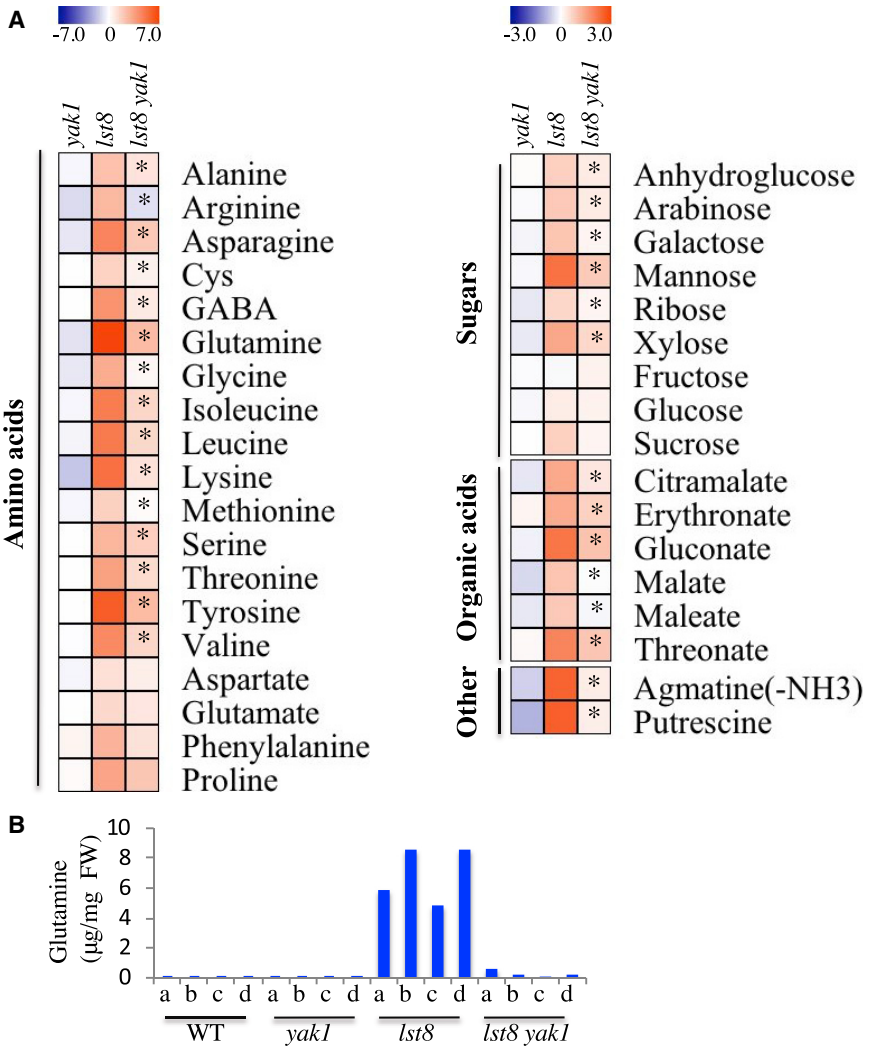


**Figure 5. Metabolite Accumulations Observed in *lst8-1-1* Are Partly Suppressed by the *Atyak1* Mutation**

(A) Seven-day-old seedlings were grown *in vitro* on *Arabidopsis* media supplemented with 0.3% sucrose under LD conditions. Heatmap depicting the $\log_2$-fold changes in metabolites of three different genotypes (*yak1* = *atyak1-4*, *lst8* = *lst8-1-1*, and *lst8 yak1* = *lst8-1-1 atyak1-4*) compared to WT. The intensities of the blue and red colors indicate, respectively, a decrease and an increase in the metabolite levels compared to WT. Asterisks show significant differences between *lst8-1-1* mutants and *lst8-1-1 atyak1-4* double mutants (n = 4, * p value < 0.05, Wilcoxon, Mann-Whitney test).

(B) Quantification of the glutamine content. Approximately 200 seedlings were used for each genotype with four biological repeats (a-d).

(Figures 6A and 6B), with 1,328 genes showing more than 2-fold changes (706 induced, 622 repressed) when compared to the WT Col-0 control. A large proportion of the differentially regulated genes in the *lst8-1-1* mutant had a lower fold change in the *lst8-1-1 atyak1-4* double mutant compared to the WT (Figure 6A). Indeed, out of 622 repressed genes in *lst8-1-1*, 403 were induced in the *lst8-1-1 atyak1-4* double mutant compared to the *lst8-1-1* mutant. Conversely, out of the 706 genes upregulated in *lst8-1-1*, 195 were downregulated in the double mutant when compared to the *lst8-1-1* mutant (Figure 6B). These results suggest that the loss of AtYAK1 activity globally dampens the impact of the *lst8-1-1* mutation on the *Arabidopsis* transcriptome.

To decipher the biological function of these genes, we first performed a gene ontology (GO) analysis on the complete set of genes whose expression was significantly altered in either *lst8-1-1* or *atyak1-4* mutants compared to the WT (Figure S6). Interestingly, genes involved in defense or salicylic acid synthesis were the most significant classes (based on false discovery rate [FDR] scores; see Figure S6) of downregulated genes in the *lst8-1-1* mutant. Conversely, these same classes of genes were enriched and upregulated in *atyak1-4.* The most significantly enriched class in *atyak1-4* downregulated genes was for transcripts involved in circadian rhythms, consistent with the described role of AtYAK1 in the regulation of the clock (Huang et al., 2017; Figure S6). We then focused on the set of genes that were differentially regulated in the *lst8-1-1* mutant and had their expression tempered or reversed in the *lst8-1-1 atyak1-4* double mutant (Figure 6C). The biological processes associated with the enriched GO terms are diverse and include root development, ion transport, as well as nutrient, stress, defense, and hormone responses (Figure 6C).

Because the hormone ABA is involved in integrating various stress signals and since *AtYAK1* as well as *LST8* are involved in ABA signaling (Kravchenko et al., 2015; Kim et al., 2016), we examined the expression of ABA-related genes in the different transcriptomes. By using the list of ABA-regulated transcripts published by Wang et al. (2018b), a significant overlap was detected between genes up- or downregulated by either ABA treatment or the *lst8-1-1* mutation (Figure 6D). Consistently, several known ABA-related genes were de-regulated in the *lst8-1-1* mutant, but this de-regulation was alleviated in *lst8-1-1 atyak1-4* when compared to *lst8-1-1* (Figure 6E). This transcriptome profiling revealed that *atyak1-4* mutations probably antagonize the ABA responses observed in *lst8-1-1* by modulating the expression of genes related to ABA.

## *AtYAK1* Mutations Suppress the ABA Hypersensitivity of the *lst8-1-1* Mutant

To further examine whether *AtYAK1* and *LST8* act together in the ABA signaling pathway, we assessed the genetic interaction of *atyak1* with the *lst8-1-1* mutant. The *atyak1* mutants

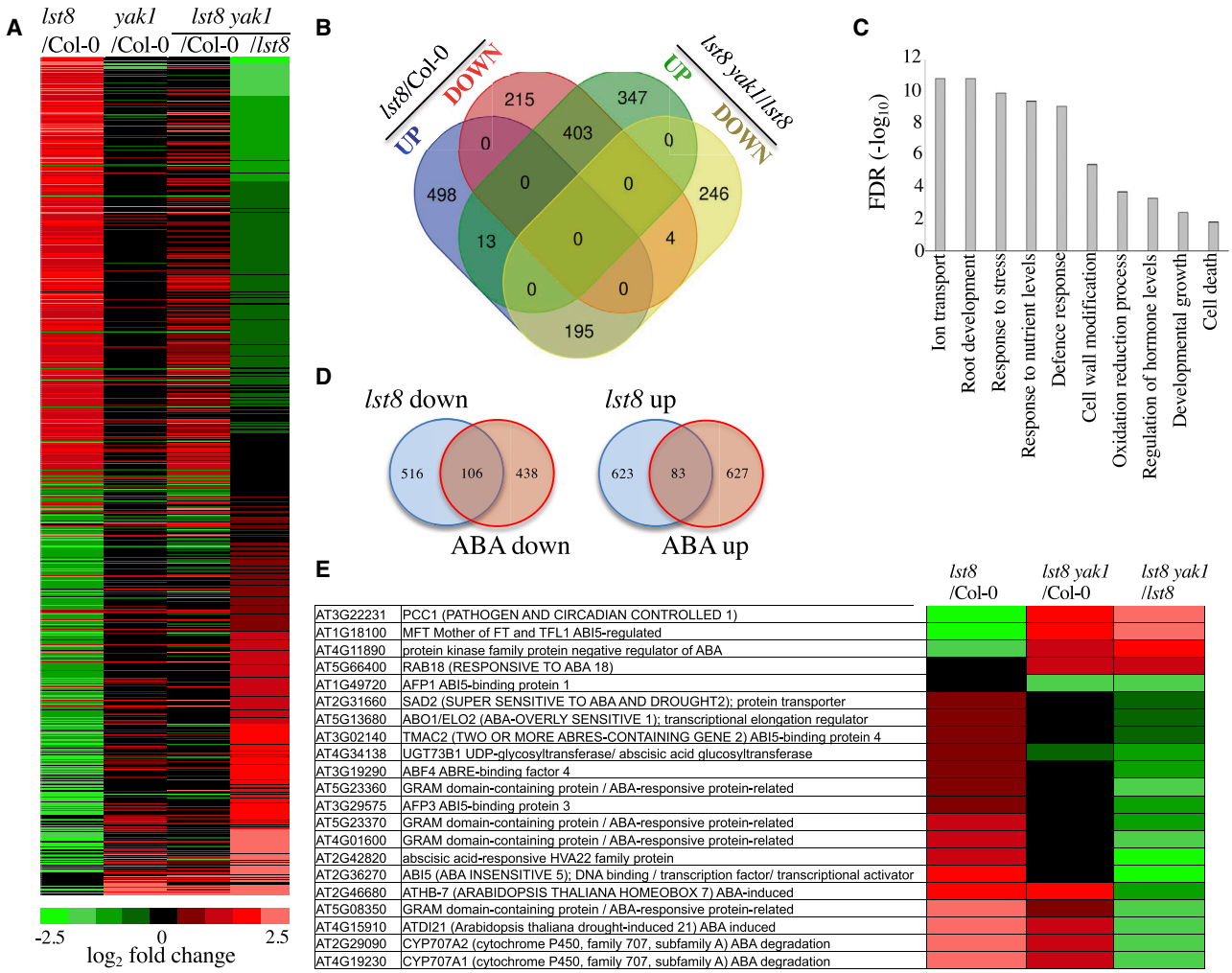


| | |
|---|---|
| AT3G22231 | PCC1 (PATHOGEN AND CIRCADIAN CONTROLLED 1) |
| AT1G18100 | MFT Mother of FT and TFL1 ABI5-regulated |
| AT4G11890 | protein kinase family protein negative regulator of ABA |
| AT5G66400 | RAB18 (RESPONSIVE TO ABA 18) |
| AT1G49720 | AFP1 ABI5-binding protein 1 |
| AT2G31660 | SAD2 (SUPER SENSITIVE TO ABA AND DROUGHT2); protein transporter |
| AT5G13680 | ABO1/ELO2 (ABA-OVERLY SENSITIVE 1); transcriptional elongation regulator |
| AT3G02140 | TMAC2 (TWO OR MORE ABRES-CONTAINING GENE 2) ABI5-binding protein 4 |
| AT4G34138 | UGT73B1 UDP-glycosyltransferase/ abscisic acid glucosyltransferase |
| AT3G19290 | ABF4 ABRE-binding factor 4 |
| AT5G23360 | GRAM domain-containing protein / ABA-responsive protein-related |
| AT3G29575 | AFP3 ABI5-binding protein 3 |
| AT5G23370 | GRAM domain-containing protein / ABA-responsive protein-related |
| AT4G01600 | GRAM domain-containing protein / ABA-responsive protein-related |
| AT2G42820 | abscisic acid-responsive HVA22 family protein |
| AT2G36270 | ABI5 (ABA INSENSITIVE 5); DNA binding / transcription factor/ transcriptional activator |
| AT2G46680 | ATHB-7 (ARABIDOPSIS THALIANA HOMEOBOX 7) ABA-induced |
| AT5G08350 | GRAM domain-containing protein / ABA-responsive protein-related |
| AT4G15910 | ATDI21 (Arabidopsis thaliana drought-induced 21) ABA induced |
| AT2G29090 | CYP707A2 (cytochrome P450, family 707, subfamily A) ABA degradation |
| AT4G19230 | CYP707A1 (cytochrome P450, family 707, subfamily A) ABA degradation |

**Figure 6. A Mutation in *AtYAK1* Partly Reduces the Variations in Gene Expression Observed in the *lst8-1-1* Mutant**

(A and B) Transcriptome analysis of the *lst8-1-1*, *atyak1-4*, and *lst8-1-1 yak1-4* double mutant by RNA-seq experiments is shown. RNA-seq data were obtained from 7-day-old seedlings grown *in vitro* under LD conditions and analyzed as described in STAR Methods.

(A) Comparisons of gene expressions were performed between each mutants and the WT Col-0 reference and between *lst8-1-1 atyak1-4* and *lst8-1-1* mutants. Differentially expressed genes were ordered from the lowest to the highest $\log_2$ ratio with the *lst8-1-1 atyak1-4*/*lst8-1-1* comparison as reference. Genes for which at least one comparison showed a differential expression (p value < 0.05) were retained.

(B) Venn diagrams showing the differentially regulated genes in common between the different comparisons ($\log_2 > |1|$). The *lst8-1-1* mutant was compared to the Col-0 reference and the *lst8-1-1 atyak1-4* double mutant was compared to *lst8-1-1*. Down and up refer to down- and upregulated genes, respectively.

(C) GO enrichment analysis. Selected enriched biological processes of the genes whose expression is significantly different (p value < 0.05 and log2 > |0.5|) in the *lst8-1-1 atyak1-4* double mutant in comparison to *lst8-1-1*.

(D) Venn diagrams showing the differentially regulated genes in common between the *lst8-1-1* mutant and ABA-treated plants. ABA RNA-seq data were from Wang et al. (2018b).

(E) Subset of ABA-related genes showing differential expression between the *lst8-1-1*/Col-0, *lst8-1-1 atyak1-4*/Col-0, and the *lst8-1-1 atyak1-4*/*lst8-1-1* comparisons. The scale for $\log_2$ ratio is shown below (A).

were shown to be hyposensitive to ABA while the *lst8-1* mutants were hypersensitive (Kravchenko et al., 2015; Kim et al., 2016). Development of the different mutants was evaluated by germinating seeds on media supplemented with DMSO (mock treatment) or ABA (1 and 2 μM). The germination and development were recorded 3, 5, 7, and 10 days after the transfer to LD conditions (Figures 7A, 7B, and S7). Figure 7B shows the germination 3 days after sowing the seeds and cotyledon establishment 7 days after germination (DAG). Three DAG, WT, *atyak1-3*, *atyak1-4*, and the two double-mutant combinations showed between 98% and 100% germination on the control media (mock), while *lst8-1-1* germination was inhibited by 60% (Figure 7B). Seed germination was inhibited by ABA for all the genotypes. However, only 4% of *lst8-1-1* seeds would germinate on ABA 2 μM compared to 50% for the other genotypes. Without ABA, 78% of *lst8-1-1* seedlings were able

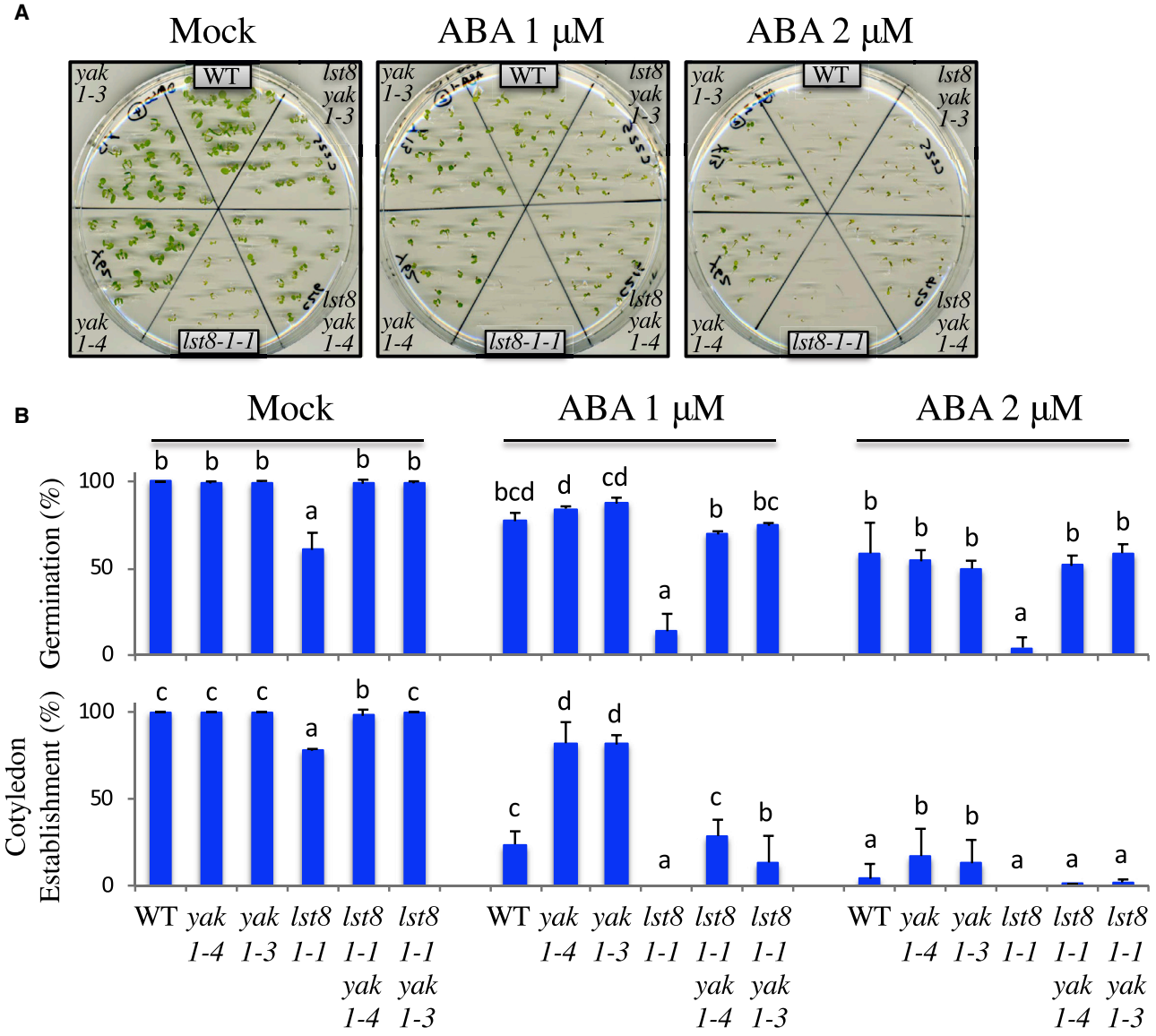


**Figure 7. Mutations in *AtYAK1* Suppress the ABA Hypersensitivity of *lst8-1-1* Mutants**

(A) Ten-day-old seedlings grown *in vitro* on half MS medium supplemented with DMSO (mock control), 1 or 2 µM of ABA. The different genotypes are WT (Col-0), *lst8-1-1*, *atyak1-3*, *atyak1-4*, *lst8-1-1 atyak1-3*, and *lst8-1-1 atyak1-4*.

(B) Quantification of the germination (3 DAG) and cotyledon establishment (7 DAG) on media supplemented with DMSO (mock control), 1 or 2 µM of ABA. Approximately 45–80 seeds were used for each genotype. Error bars indicate the standard deviation of three independent experiments. Letters indicate significantly different classes (non-parametric Kruskal-Wallis test, $p < 0.05$).

to expand cotyledons 7 DAG, compared to 98%–100% for the other genotypes. While the presence of ABA delayed the development of all genotypes, growth of *lst8-1-1* was arrested by ABA (Figure 7B). *Atyak1* mutants were less sensitive to ABA than WT since 81% of both *atyak1* mutant seeds developed cotyledons on 1 µM ABA, compared to 24% for WT plants or 29%–13% for the double mutants. The *lst8-1-1 atyak1* double mutants behaved similarly to WT in the presence of ABA. These results indicate that *atyak1* mutations dampen ABA sensitivity in *lst8-1-1*.

## DISCUSSION

In this study we isolated two suppressors of the *lst8-1-1* mutant, which contained loss-of-function mutations in the *AtYAK1* (At5g35980) gene. The LST8 protein is already known to interact with the plant TORC1 complex. We further showed that LST8 is required for the sugar-induced TOR activation. However, loss of AtYAK1 did not restore TOR activity, suggesting that AtYAK1 could be a TOR effector. Our genetic analysis implied that AtYAK1 and TOR act in a common pathway to

control plant growth. This notion is further supported by the fact that RAPTOR and AtYAK1 physically interact and loss of AtYAK1 confers resistance to the specific TOR inhibitor AZD-8055. The AtYAK1 protein interacts with RAPTOR both in a yeast two-hybrid and *in planta* BiFC experiments. On the contrary no interaction with LST8 was detected using these same techniques. Nevertheless, Van Leene et al. (2019) identified AtYAK1 in an immunopurification experiment using tagged LST8 as bait. This suggests that AtYAK1 interacts with the RAPTOR component of the TORC1 complex, which also contains LST8. Van Leene et al. (2019) showed that AtYAK1 is phosphorylated on two conserved Ser residues in a TOR-dependent way and we further demonstrate that TOR-containing fractions are able to phosphorylate AtYAK1 *in vitro*. This is the first evidence in eukaryotes that TOR is able to phosphorylate the conserved AtYAK1 kinase. It is tempting to suggest that TORC1 binds to AtYAK1 and inactivates it by phosphorylation since loss of AtYAK1 alleviates the effects of TOR inhibition in the *lst8-1-1* mutant.

YAK1 is the founding member of the conserved DYRK protein kinase family and has orthologs in lower eukaryotes and plants (Aranda et al., 2011; Figure S2B). In yeast, YAK1 inhibits cell proliferation and stimulates stress responses in order to promote cell survival (Garrett et al., 1991; Malcher et al., 2011). In response to glucose availability, the yeast cyclic AMP (cAMP) regulated protein kinase A (PKA) phosphorylates YAK1 and inhibits its relocation into the nucleus, while rapamycin treatment or PKA inhibition results in the nuclear localization of YAK1 (Schmelzle et al., 2004; Lee et al., 2011). The deletion of YAK1 reverts the growth defect of yeast cells lacking PKA activity (Garrett and Broach, 1989). Once in the nucleus, YAK1 leads to the activation of stress-responsive transcription factors like Hsf1, Msn2, and Msn4 (Lee et al., 2008). As in yeast, where YAK1 transduces the perception of stresses, we can hypothesize that AtYAK1 also conveys stress signals in *Arabidopsis*. In support of this model, the GO classification (Figure S6) suggests that the AtYAK1-regulated genes were related to stress and defense. Therefore, we propose a model where AtYAK1 mediates stress signals in *Arabidopsis* by blocking growth and needs to be inhibited by TOR in order to activate plant growth.

DYRKs can phosphorylate Ser (S), Thr (T), and Tyr (Y) residues. They become activated by autophosphorylation of the second Y residue located in their conserved activation loop motif Yx(P)Y. The nonsense mutation in the *sol23* suppressor line preserves this activation loop (YSY in *Arabidopsis*) but results in the deletion of the C-terminal part of the conserved DYRK kinase domain (Figure S2A). Interestingly, phosphorylation of the regulatory Y residue in the AtYAK1 activation loop was found to be highly increased by ABA treatment (Kline et al., 2010). This indicates that AtYAK1 activity could be modulated in response to ABA levels. Here, we show that *atyak1* mutations suppressed the ABA hypersensitivity of *lst8-1-1* mutants, suggesting that TOR may act through AtYAK1 to repress ABA signaling. TOR silenced lines or TORC1 mutants were already shown to be hypersensitive to ABA (Deprost et al., 2007; Kravchenko et al., 2015; Salem et al., 2018). Moreover, TOR was shown to reduce ABA responses by phosphorylation of the ABA PYL receptors (Wang et al., 2018a). AtYAK1 can also phosphorylate annexins (Kim et al., 2015), which are involved in ABA signaling (Lee et al., 2004). Annexins are $Ca^{2+}$-dependent membrane-binding proteins. Taken together, we propose that during favorable growth conditions TOR would negatively control ABA signaling by inhibition of the AtYAK1 activity.

TOR has been shown to integrate light, sugar, auxin, cytokinin, and brassinosteroid signals (Dobrenel et al., 2016a). AtYAK1 interacts with the light-regulated WD-repeat 1 (LWD1) protein and was found to regulate light responses such as the circadian clock, photomorphogenesis, and flowering (Huang et al., 2017). The *atyak1* mutation compensates the early flowering phenotype of *lwd1* mutants but in our study it partly suppressed the late flowering phenotype of *lst8-1-1*. Huang et al. also proposed that AtYAK1 is an inducer of light responses since *atyak1* had reduced light responses with longer hypocotyls than WT. Accordingly, *atyak1* mutations rescued the short hypocotyl phenotype of *lst8-1-1* mutants. Because *lst8-1-1* mutants are also hypersensitive to an increase in day length (Moreau et al., 2012), the loss of AtYAK1 activity could contribute to the reduction in light sensitivity of *lst8-1-1.*

One of the hallmarks of TOR inhibition in plants is the accumulation of amino acids (Moreau et al., 2012; Mubeen et al., 2018). Recent work by Mubeen et al. (2018) suggested that this increase in amino acid levels occurring when TOR is inhibited is due to an increased nitrogen uptake followed by its assimilation into amino acid. Since in our study *atyak1* mutations suppressed the amino acid accumulation observed in *lst8-1-1* plants, we checked whether genes involved in nitrogen uptake were regulated by AtYAK1 or LST8 (Figure S7B). Contrary to what could have been expected, genes encoding nitrate and ammonium transporters (NRT2 and AMT families, respectively) were repressed in the *lst8-1-1* mutant and re-induced by the *atyak1* mutation. This could be the consequence of a negative feedback in response to the excess of amino acids. Furthermore, yeast YAK1 targets transcription factors and transcriptional coregulators, which regulate stress responses (Lee et al., 2008; Malcher et al., 2011), or ribosome biogenesis and the mRNA life cycle (Martin et al., 2004; Moriya et al., 2001). In *Arabidopsis*, *atyak1* mutants were also identified in a screen for AZD-8055-resistant *Arabidopsis* plants (Barrada et al., 2019). In this recent report AtYAK1 was shown to control root meristem functions and to upregulate SIAMESE-related proteins which inhibit cyclin-dependent kinases (Barrada et al., 2019). Future work will thus be necessary to identify AtYAK1 targets in order to further investigate how this kinase controls plant growth.

In conclusion, we uncovered the AtYAK1 kinase as a suppressor of TORC1 mutations and as a TOR target. Upon TOR inhibition, our results support the hypothesis that AtYAK1 inhibits growth, increases ABA sensitivity, and reprograms the plant gene expression and metabolism. A tight control of AtYAK1 by TOR is probably essential for plant growth to proceed. Many hormone and stress signaling pathways are known to regulate plant growth. It remains to be shown how TOR and AtYAK1 integrate these different signaling pathways.

## STAR★METHODS

Detailed methods are provided in the online version of this paper and include the following:

- KEY RESOURCES TABLE
- CONTACT FOR REAGENT AND RESOURCE SHARING
- EXPERIMENTAL MODEL AND SUBJECT DETAILS
  - Plant Lines
- METHOD DETAILS
  - Suppressor Screen
  - Plant Growth Conditions
  - Western Blotting
  - Yeast Two-Hybrid Assays
  - Bimolecular Fluorescence Complementation (BiFC) Assay in Nicotiana Benthamiana Leaves
  - *In Vitro* Kinase Assay
  - Transcriptome Studies
  - Metabolite Measurements
  - Metabolic Data Processing
- QUANTIFICATION AND STATISTICAL ANALYSIS
  - RNA-Seq Bioinformatic Treatment and Analysis
  - Metabolite Absolute Quantification
  - Growth Data Analysis
- DATA AND SOFTWARE AVAILABILITY
  - RNA-Seq Data
  - Metabolomic Data

## SUPPLEMENTAL INFORMATION

Supplemental Information can be found online at https://doi.org/10.1016/j.celrep.2019.05.074.

## ACKNOWLEDGMENTS

We are indebted to Prof. Christophe Robaglia's laboratory and Dr. Anne Krapp for valuable and informative discussions. We wish to thank members of the Plant Observatory-Plant Culture platform for taking excellent care of the plants. Work in our laboratory was partly funded by DecoraTOR ANR grant ANR14-CE19-007 to C.M., C.F., and A.-S.L. This work has also benefited from a French State grant (LabEx Saclay Plant Sciences-SPS ANR-10-LABX-0040-SPS), managed by the French National Research Agency under an "Investments for the Future" program (ANR-11-IDEX-0003-02) to C.M. and C.F. G.T.D. was supported by a grant from INRA and from the Agreen-Skills+ EU fellowship program (FP7- 609398).

## AUTHOR CONTRIBUTIONS

C.F., G.T.D., and J.V.L. designed and conducted the experiments; G.C., S.H., S.P.-L.-R., and R.M. developed the methodology and ran analyses; G.D.J., A.-S.L., and C.M. designed and supervised the experiments; and C.F., A.-S.L., and C.M directed the study and wrote the first draft of the manuscript. All authors provided comments on and approved the manuscript.

## DECLARATION OF INTERESTS

The authors declare no competing interests.

Received: November 25, 2018
Revised: April 26, 2019
Accepted: May 20, 2019
Published: June 18, 2019

## REFERENCES

Ahn, C.S., Han, J.A., Lee, H.S., Lee, S., and Pai, H.S. (2011). The PP2A regulatory subunit Tap46, a component of the TOR signaling pathway, modulates growth and metabolism in plants. Plant Cell *23*, 185–209.

Albert, V., and Hall, M.N. (2015). mTOR signaling in cellular and organismal energetics. Curr. Opin. Cell Biol. *33*, 55–66.

Aranda, S., Laguna, A., and de la Luna, S. (2011). DYRK family of protein kinases: evolutionary relationships, biochemical properties, and functional roles. FASEB J. *25*, 449–462.

Aylett, C.H., Sauer, E., Imseng, S., Boehringer, D., Hall, M.N., Ban, N., and Maier, T. (2016). Architecture of human mTOR complex 1. Science *351*, 48–52.

Azimzadeh, J., Nacry, P., Christodoulidou, A., Drevensek, S., Camilleri, C., Amiour, N., Parcy, F., Pastuglia, M., and Bouchez, D. (2008). Arabidopsis TONNEAU1 proteins are essential for preprophase band formation and interact with centrin. Plant Cell *20*, 2146–2159.

Baena-González, E., and Hanson, J. (2017). Shaping plant development through the SnRK1-TOR metabolic regulators. Curr. Opin. Plant Biol. *35*, 152–157.

Baretić, D., and Williams, R.L. (2014). The structural basis for mTOR function. Semin. Cell Dev. Biol. *36*, 91–101.

Barrada, A., Djendli, M., Desnos, T., Mercier, R., Robaglia, C., Montané, M.H., and Menand, B. (2019). A TOR-YAK1 signaling axis controls cell cycle, meristem activity and plant growth in *Arabidopsis*. Development *146*, dev171298.

Berendzen, K., Searle, I., Ravenscroft, D., Koncz, C., Batschauer, A., Coupland, G., Somssich, I.E., and Ülker, B. (2005). A rapid and versatile combined DNA/RNA extraction protocol and its application to the analysis of a novel DNA marker set polymorphic between Arabidopsis thaliana ecotypes Col-0 and Landsberg erecta. Plant Methods *1*, 4.

Blenis, J. (2017). TOR, the Gateway to Cellular Metabolism, Cell Growth, and Disease. Cell *171*, 10–13.

Bolger, A.M., Lohse, M., and Usadel, B. (2014). Trimmomatic: a flexible trimmer for Illumina sequence data. Bioinformatics *30*, 2114–2120.

Deprost, D., Yao, L., Sormani, R., Moreau, M., Leterreux, G., Nicolaï, M., Bedu, M., Robaglia, C., and Meyer, C. (2007). The Arabidopsis TOR kinase links plant growth, yield, stress resistance and mRNA translation. EMBO Rep. *8*, 864–870.

Díaz-Troya, S., Florencio, F.J., and Crespo, J.L. (2008). Target of rapamycin and LST8 proteins associate with membranes from the endoplasmic reticulum in the unicellular green alga Chlamydomonas reinhardtii. Eukaryot. Cell *7*, 212–222.

Dobrenel, T., Caldana, C., Hanson, J., Robaglia, C., Vincentz, M., Veit, B., and Meyer, C. (2016a). TOR Signaling and Nutrient Sensing. Annu. Rev. Plant Biol. *67*, 261–285.

Dobrenel, T., Mancera-Martínez, E., Forzani, C., Azzopardi, M., Davanture, M., Moreau, M., Schepetilnikov, M., Chicher, J., Langella, O., Zivy, M., et al. (2016b). The Arabidopsis TOR Kinase Specifically Regulates the Expression of Nuclear Genes Coding for Plastidic Ribosomal Proteins and the Phosphorylation of the Cytosolic Ribosomal Protein S6. Front. Plant Sci. *7*, 1611.

Edgar, R., Domrachev, M., and Lash, A.E. (2002). Gene Expression Omnibus: NCBI gene expression and hybridization array data repository. Nucleic Acids Res. *30*, 207–210.

Estelle, M.A., and Somerville, C. (1987). Auxin-resistant mutants of Arabidopsis thaliana with an altered morphology. Mol. Gen. Genet. *206*, 200–206.

Gagnot, S., Tamby, J.P., Martin-Magniette, M.L., Bitton, F., Taconnat, L., Balzergue, S., Aubourg, S., Renou, J.P., Lecharny, A., and Brunaud, V. (2008). CATdb: a public access to Arabidopsis transcriptome data from the URGV-CATMA platform. Nucleic Acids Res. *36*, D986–D990.

Garrett, S., and Broach, J. (1989). Loss of Ras activity in Saccharomyces cerevisiae is suppressed by disruptions of a new kinase gene, YAKI, whose product may act downstream of the cAMP-dependent protein kinase. Genes Dev. *3*, 1336–1348.

Garrett, S., Menold, M.M., and Broach, J.R. (1991). The Saccharomyces cerevisiae YAK1 gene encodes a protein kinase that is induced by arrest early in the cell cycle. Mol. Cell. Biol. *11*, 4045–4052.

Gietz, D., St Jean, A., Woods, R.A., and Schiestl, R.H. (1992). Improved method for high efficiency transformation of intact yeast cells. Nucleic Acids Res. *20*, 1425.

Girard, C., Crismani, W., Froger, N., Mazel, J., Lemhemdi, A., Horlow, C., and Mercier, R. (2014). FANCM-associated proteins MHF1 and MHF2, but not the other Fanconi anemia factors, limit meiotic crossovers. Nucleic Acids Res. *42*, 9087–9095.

Granier, F., Lemaire, A., Antelme, S., Vogel, J., and Sibout, R. (2016). Chemical and radiation mutagenesis: Induction and detection by whole genome sequencing. In Genetics and Genomics of Brachypodium, J. Vogel, ed. (Springer), pp. 155–170.

Huang, W.Y., Wu, Y.C., Pu, H.Y., Wang, Y., Jang, G.J., and Wu, S.H. (2017). Plant dual-specificity tyrosine phosphorylation-regulated kinase optimizes light-regulated growth and development in Arabidopsis. Plant Cell Environ. *40*, 1735–1747.

James, P., Halladay, J., and Craig, E.A. (1996). Genomic libraries and a host strain designed for highly efficient two-hybrid selection in yeast. Genetics *144*, 1425–1436.

Kim, D., Ntui, V.O., Zhang, N., and Xiong, L. (2015). Arabidopsis Yak1 protein (AtYak1) is a dual specificity protein kinase. FEBS Lett. *589*, 3321–3327.

Kim, D., Ntui, V.O., and Xiong, L. (2016). Arabidopsis YAK1 regulates abscisic acid response and drought resistance. FEBS Lett. *590*, 2201–2209.

Kline, K.G., Barrett-Wilt, G.A., and Sussman, M.R. (2010). In planta changes in protein phosphorylation induced by the plant hormone abscisic acid. Proc. Natl. Acad. Sci. USA *107*, 15986–15991.

Kopylova, E., Noé, L., and Touzet, H. (2012). SortMeRNA: fast and accurate filtering of ribosomal RNAs in metatranscriptomic data. Bioinformatics *28*, 3211–3217.

Kravchenko, A., Citerne, S., Jéhanno, I., Bersimbaev, R.I., Veit, B., Meyer, C., and Leprince, A.S. (2015). Mutations in the Arabidopsis Lst8 and Raptor genes encoding partners of the TOR complex, or inhibition of TOR activity decrease abscisic acid (ABA) synthesis. Biochem. Biophys. Res. Commun. *467*, 992–997.

Langmead, B., Trapnell, C., Pop, M., and Salzberg, S.L. (2009). Ultrafast and memory-efficient alignment of short DNA sequences to the human genome. Genome Biol. *10*, R25.

Lee, P., Cho, B.R., Joo, H.S., and Hahn, J.S. (2008). Yeast Yak1 kinase, a bridge between PKA and stress-responsive transcription factors, Hsf1 and Msn2/Msn4. Mol. Microbiol. *70*, 882–895.

Lee, P., Paik, S.M., Shin, C.S., Huh, W.K., and Hahn, J.S. (2011). Regulation of yeast Yak1 kinase by PKA and autophosphorylation-dependent 14-3-3 binding. Mol. Microbiol. *79*, 633–646.

Lee, S., Lee, E.J., Yang, E.J., Lee, J.E., Park, A.R., Song, W.H., and Park, O.K. (2004). Proteomic identification of annexins, calcium-dependent membrane binding proteins that mediate osmotic stress and abscisic acid signal transduction in Arabidopsis. Plant Cell *16*, 1378–1391.

Li, X., Cai, W., Liu, Y., Li, H., Fu, L., Liu, Z., Xu, L., Liu, H., Xu, T., and Xiong, Y. (2017). Differential TOR activation and cell proliferation in *Arabidopsis* root and shoot apexes. Proc. Natl. Acad. Sci. USA *114*, 2765–2770.

Lu, Q., Tang, X., Tian, G., Wang, F., Liu, K., Nguyen, V., Kohalmi, S.E., Keller, W.A., Tsang, E.W.T., Harada, J.J., et al. (2010). Arabidopsis homolog of the yeast TREX-2 mRNA export complex: components and anchoring nucleoporin. Plant J. *61*, 259–270.

Maegawa, K., Takii, R., Ushimaru, T., and Kozaki, A. (2015). Evolutionary conservation of TORC1 components, TOR, Raptor, and LST8, between rice and yeast. Mol. Genet. Genomics *290*, 2019–2030.

Mahfouz, M.M., Kim, S., Delauney, A.J., and Verma, D.P. (2006). Arabidopsis TARGET OF RAPAMYCIN interacts with RAPTOR, which regulates the activity of S6 kinase in response to osmotic stress signals. Plant Cell *18*, 477–490.

Malcher, M., Schladebeck, S., and Mösch, H.U. (2011). The Yak1 protein kinase lies at the center of a regulatory cascade affecting adhesive growth and stress resistance in Saccharomyces cerevisiae. Genetics *187*, 717–730.

Martin, D.E., Soulard, A., and Hall, M.N. (2004). TOR regulates ribosomal protein gene expression via PKA and the Forkhead transcription factor FHL1. Cell *119*, 969–979.

McCarthy, D.J., Chen, Y., and Smyth, G.K. (2012). Differential expression analysis of multifactor RNA-Seq experiments with respect to biological variation. Nucleic Acids Res. *40*, 4288–4297.

Montané, M.H., and Menand, B. (2013). ATP-competitive mTOR kinase inhibitors delay plant growth by triggering early differentiation of meristematic cells but no developmental patterning change. J. Exp. Bot. *64*, 4361–4374.

Moreau, M., Azzopardi, M., Clément, G., Dobrenel, T., Marchive, C., Renne, C., Martin-Magniette, M.L., Taconnat, L., Renou, J.P., Robaglia, C., and Meyer, C. (2012). Mutations in the Arabidopsis homolog of LST8/GβL, a partner of the target of Rapamycin kinase, impair plant growth, flowering, and metabolic adaptation to long days. Plant Cell *24*, 463–481.

Moriya, H., Shimizu-Yoshida, Y., Omori, A., Iwashita, S., Katoh, M., and Sakai, A. (2001). Yak1p, a DYRK family kinase, translocates to the nucleus and phosphorylates yeast Pop2p in response to a glucose signal. Genes Dev. *15*, 1217–1228.

Mubeen, U., Jüppner, J., Alpers, J., Hincha, D.K., and Giavalisco, P. (2018). Target of Rapamycin inhibition in Chlamydomonas reinhardtii triggers de novo amino acid synthesis by enhancing nitrogen assimilation. Plant Cell *30*, 2240–2254.

Nukarinen, E., Nägele, T., Pedrotti, L., Wurzinger, B., Mair, A., Landgraf, R., Börnke, F., Hanson, J., Teige, M., Baena-Gonzalez, E., et al. (2016). Quantitative phosphoproteomics reveals the role of the AMPK plant ortholog SnRK1 as a metabolic master regulator under energy deprivation. Sci. Rep. *6*, 31697.

Ogawa, Y., Nonaka, Y., Goto, T., Ohnishi, E., Hiramatsu, T., Kii, I., Yoshida, M., Ikura, T., Onogi, H., Shibuya, H., et al. (2010). Development of a novel selective inhibitor of the Down syndrome-related kinase Dyrk1A. Nat. Commun. *1*, 86.

Pfeiffer, A., Janocha, D., Dong, Y., Medzihradszky, A., Schöne, S., Daum, G., Suzaki, T., Forner, J., Langenecker, T., Rempel, E., et al. (2016). Integration of light and metabolic signals for stem cell activation at the shoot apical meristem. eLife *5*, e17023.

R Development Core Team (2005). R: A language and environment for statistical computing, reference index version 2.2.1 (R Foundation for Statistical Computing). http://www.R-project.org.

Rexin, D., Meyer, C., Robaglia, C., and Veit, B. (2015). TOR signalling in plants. Biochem. J. *470*, 1–14.

Rigaill, G., Balzergue, S., Brunaud, V., Blondet, E., Rau, A., Rogier, O., Caius, J., Maugis-Rabusseau, C., Soubigou-Taconnat, L., Aubourg, S., et al. (2018). Synthetic data sets for the identification of key ingredients for RNA-seq differential analysis. Brief. Bioinform. *19*, 65–76.

Roberg, K.J., Bickel, S., Rowley, N., and Kaiser, C.A. (1997). Control of amino acid permease sorting in the late secretory pathway of Saccharomyces cerevisiae by SEC13, LST4, LST7 and LST8. Genetics *147*, 1569–1584.

Salem, M.A., Li, Y., Bajdzienko, K., Fisahn, J., Watanabe, M., Hoefgen, R., Schöttler, M.A., and Giavalisco, P. (2018). RAPTOR Controls Developmental Growth Transitions by Altering the Hormonal and Metabolic Balance. Plant Physiol. *177*, 565–593.

Schepetilnikov, M., Makarian, J., Srour, O., Geldreich, A., Yang, Z., Chicher, J., Hammann, P., and Ryabova, L.A. (2017). GTPase ROP2 binds and promotes activation of target of rapamycin, TOR, in response to auxin. EMBO J. *36*, 886–903.

Schmelzle, T., Beck, T., Martin, D.E., and Hall, M.N. (2004). Activation of the RAS/cyclic AMP pathway suppresses a TOR deficiency in yeast. Mol. Cell. Biol. *24*, 338–351.

Shi, L., Wu, Y., and Sheen, J. (2018). TOR signaling in plants: conservation and innovation. Development *145*, dev160887.

Smith, T.F., Gaitatzes, C., Saxena, K., and Neer, E.J. (1999). The WD repeat: a common architecture for diverse functions. Trends Biochem. Sci. *24*, 181–185.

Thimm, O., Bläsing, O., Gibon, Y., Nagel, A., Meyer, S., Krüger, P., Selbig, J., Müller, L.A., Rhee, S.Y., and Stitt, M. (2004). MAPMAN: a user-driven tool to display genomics data sets onto diagrams of metabolic pathways and other biological processes. Plant J. *37*, 914–939.

Van Leene, J., Han, C., Gadeyne, A., Eeckhout, D., Matthijs, C., Cannoot, B., De Winne, N., Persiau, G., Van De Slijke, E., Van de Cotte, B., et al. (2019). Capturing the phosphorylation and protein interaction landscape of the plant TOR kinase. Nat. Plants *5*, 316–327.

Wang, P., Zhao, Y., Li, Z., Hsu, C.C., Liu, X., Fu, L., Hou, Y.J., Du, Y., Xie, S., Zhang, C., et al. (2018a). Reciprocal Regulation of the TOR Kinase and ABA Receptor Balances Plant Growth and Stress Response. Mol. Cell *69*, 100–112.e6.

Wang, H., Tang, J., Liu, J., Hu, J., Liu, J., Chen, Y., Cai, Z., and Wang, X. (2018b). Abscisic Acid Signaling Inhibits Brassinosteroid Signaling through Dampening the Dephosphorylation of BIN2 by ABI1 and ABI2. Mol. Plant *11*, 315–325.

Wullschleger, S., Loewith, R., and Hall, M.N. (2006). TOR signaling in growth and metabolism. Cell *124*, 471–484.

Xiong, Y., McCormack, M., Li, L., Hall, Q., Xiang, C., and Sheen, J. (2013). Glucose-TOR signalling reprograms the transcriptome and activates meristems. Nature *496*, 181–186.

Yang, H., Rudge, D.G., Koos, J.D., Vaidialingam, B., Yang, H.J., and Pavletich, N.P. (2013). mTOR kinase structure, mechanism and regulation. Nature *497*, 217–223.

Zhang, Z., Zhu, J.Y., Roh, J., Marchive, C., Kim, S.K., Meyer, C., Sun, Y., Wang, W., and Wang, Z.Y. (2016). TOR Signaling Promotes Accumulation of BZR1 to Balance Growth with Carbon Availability in Arabidopsis. Curr. Biol. *26*, 1854–1860.

# STAR★METHODS

## KEY RESOURCES TABLE

| REAGENT or RESOURCE | SOURCE | IDENTIFIER |
|---|---|---|
| Antibodies | | |
| Anti-RPS6 rabbit polyclonal antibody | Dobrenel et al., 2016b | N/A |
| Anti-phosphorylated RPS6 rabbit polyclonal antibody | Dobrenel et al., 2016b | N/A |
| Anti-rabbit HRP-conjugated | SIGMA-Aldrich | Cat# A0545; RRID: AB_257896 |
| Clarity Western ECL blotting substrate | Bio-Rad | Cat# 1705061 |
| Yeast Strains and plasmids | | |
| PJ69-4A | James et al., 1996 | N/A |
| pGBKT7-GW | Lu et al., 2010 | N/A |
| pGADT7-GW | Lu et al., 2010 | N/A |
| Bacterial strains and plasmids | | |
| *Agrobacterium tumefaciens* C58C1-pMP90 | Moreau et al., 2012 | N/A |
| pBIPF1-4 | Azimzadeh et al., 2008 | N/A |
| pDEST-His-MBP | Addgene | Cat# 11085; RRID: Addgene_11085 |
| Chemicals | | |
| AZD-8055 | Sellekchem | Cat# S1555 |
| Murashige and Skoog medium | Duchefa | Cat# M0222 |
| Phytagel | SIGMA-Aldrich | Cat# P8169 |
| Critical Commercial Assays | | |
| Nucleospin Plant II DNA extraction kit | Macherey-Nagel | Cat# 740770 |
| Deposited Data | | |
| RNA-sequencing | This paper | GEO: GSE120003 |
| Experimental Models: Organisms/Strains | | |
| *Arabidopsis thaliana* Col0 | Versailles Stock Center | Col0 |
| Oligonucleotides | | |
| CAPS: TTTGGCCAACTTGCGTTAACT | Eurofins | N/A |
| For CAPS: ATACCCTAGTATTTCA ATCATACGC | Eurofins | N/A |
| Rev Actin: GCCATCCAAGCTGTTCTCTC | Eurofins | N/A |
| For Actin: CCCTCGTAGATTGGCACAGT | Eurofins | N/A |
| Rev Yak-1F: CACTATTTCCAGGAGGTTCAGA | Eurofins | N/A |
| Yak-1R: TGACCAACGTTTTGCTGGAT | Eurofins | N/A |
| Yak-2F: GCAAAGCACCCTTTCATTACT | Eurofins | N/A |
| Yak-2R: ATTGCCAGTCCCTCCATAGC | Eurofins | N/A |
| LBsail: TAGCATCTGAATTTCATAACCAATCTCGATACAC | Eurofins | N/A |
| LB1-3: ATTTTGCCGATTTCGGAAC | Eurofins | N/A |
| Software and Algorithms | | |
| XL-STAT | XLSTAT | N/A |
| Mutdetect | Granier et al., 2016 | N/A |

## CONTACT FOR REAGENT AND RESOURCE SHARING

Further information and requests for resources and reagents should be directed to and will be fulfilled by the Lead Contact, Dr. Christian Meyer (christian.meyer@inra.fr). There are no restrictions on reagent sharing to disclose.

## EXPERIMENTAL MODEL AND SUBJECT DETAILS

### Plant Lines

The *Arabidopsis thaliana* ecotype Columbia 0 was used for all the experiments and grown as previously described (Moreau et al., 2012). The *lst8-1-1*, *lst8-1-2* and *atyak1-3* (Salk_02459, Sail_641_D10, Salk_131306 respectively) mutant lines have been previously described (Moreau et al., 2012; Huang et al., 2017). The loss-of-function mutant lines *atyak1-4* (Sail_627_C09) and *yak1-5* (Sail_1219_F01C01) were obtained from the Nottingham *Arabidopsis* stock center. T-DNA insertions for each mutant line were confirmed by sequencing and genotyping. Primers used for the genotyping are listed in Table S1 and in the Key Resources Table. *Nicotiana benthamiana* was grown in a greenhouse with standard nutrition.

## METHOD DETAILS

### Suppressor Screen

20 000 *lst8-1-1* seeds were treated with 10 mL of 0.35% ethyl methanesulfonate (EMS v/v) for 17 h at room temperature. The mutagen was neutralized by adding 10 mL of sodium thiosulfate 1M for 5 min. Seeds were then washed 6 times with 15 mL of water for 15 min and sown in soil. Since the *lst8-1-1* mutant shows low fertility and sensitivity to long days (LD), the mutagenized seeds were grown in short days (10h light) and after 50 days flowering was induced with 10 days of LD (14 h light) before returning the plants to short day conditions. 1500 M1 plants were recovered and harvested in 250 pools of 6 plants each. M2 plants of each pool were screened for their ability to grow faster than *lst8-1-1*. Genomic DNA was extracted with the NucleoSpin Plant II Kit (Macherey-Nagel) from the flowers of M2 plants. The DNA was sequenced by the GetPlaGe Genotoul sequencing platform (Toulouse, France) using the Illumina Hiseq 3000 sequencing system. Mutations were identified by using the MutDetect pipeline (Girard et al., 2014; Granier et al., 2016). A list of SNPs was created by using as reference genome TAIR10. The lists of non-sense/strong (new stop or start codons, loss of start codon, splice site changes) mutations for the *sol23* and *sol69* suppressor lines are provided in Data S1.

To confirm the causal mutation in *sol23,* the mutation (G924A in *YAK1* At5g35980) was genotyped using a CAPS (cleaved amplified polymorphic sequence) assay. CAPS primers were designed using dCAPS Finder 2.0 (Table S1). *sol23* M2 suppressor plants were backcrossed to *lst8-1-1*. In the F2 population *sol23* mutation segregates at a single locus and is recessive (Figures S1D and S1E). Genomic DNA was extracted from the segregating F2 population by grinding a leaf in a sucrose solution (50 mM Tris-HCL pH 7.5, 300 mM NaCl, 300 mM sucrose) and by heating the extract at 95°C for 10 min (Berendzen et al., 2005). 1.5 μl of genomic DNA was used as a template for the PCR reaction. Ten μl of the PCR reactions were digested for 3 h with the MboI restriction enzyme (2.5 units) in a total volume of 20 μl at 37°C. The DNA fragments were subsequently separated by gel electrophoresis (2% agarose gel).

### Plant Growth Conditions

Seeds were germinated on two different media: *Arabidopsis* medium (1.8 g $L^{-1}$ *Arabidopsis* medium including vitamins (Estelle and Somerville, 1987), 0.3% sucrose, 0.5 g $L^{-1}$ 2-(N-Morpholino) ethanesulfonic acid sodium salt (MES) pH 5.7 and 0.5% phytagel) or 0.5xMS medium (2.2 g $L^{-1}$ Murashige Skoog including vitamins (Duchefa, M0222), 0.3% sucrose, 0.5 g $L^{-1}$ MES pH 5.8 and 0.5% phytagel). The seeds were stratified at 4°C between 48 and 72 h and were then transferred to 20°C under long day conditions (16 h light, 8 h dark) for germination and growth. Four-day-old seedlings were then transferred onto *Arabidopsis* medium grown either vertically for 7 days or grown horizontally for 14 days before measuring the root length or the fresh weight, respectively. For AZD-8055 (Selleckchem, S1555) treatment, 4-day-old seedlings were transferred onto *Arabidopsis* medium containing either 5 μl DMSO (Mock treatment) or 0.5 or 1 μM AZD-8055 (dissolved in DMSO) and were grown vertically. Root length was marked 3, 5 and 7 days after transfer (DAT).

Hypocotyl measurements were performed in the dark. Seeds were sown on *Arabidopsis* medium, stratified for 72 h before exposing to light for 3 h and then grown vertically in the dark for 6 days. Root and hypocotyl length were measured using ImageJ software. For sucrose treatments 6-day-old seedlings grown on MS medium were transferred to MS liquid sugar-free medium for 24 h and then either mock or sugar treated (0.5%) for 4 h.

For the metabolite and the RNaseq analysis 7-day-old seedlings grown on *Arabidopsis* medium were harvested. 200 seedlings were collected for each lines (WT Col-0, *atyak1-4, lst8-1-1, lst8-1-1 atyak1-4*) and frozen in liquid nitrogen before grinding. The ABA effect on germination and early development assay was performed on 0.5xMS medium supplemented with either DMSO (mock treatment) or ABA at final concentrations of 1 or 2 μM. At least 45 to 80 seeds of each genotype were used. Two developmental stages were scored, as follows: *1)* Germination, protrusion of the radicle and *2)* cotyledon establishment, when the cotyledons were green and open. The germination and development were recorded 3, 5, 7 and 10 days after the transfer to long day conditions.

### Western Blotting

Proteins were extracted from 7-day-old *Arabidopsis* seedlings by grinding them in Laemmli buffer (62.5 mM Tris-HCL pH 6.8, 2% SDS, 100 mM dithiothreitol (DTT), 10% glycerol, 0.1% Triton X-100 (v/v), 0.0025% bromophenol blue). Total protein extracts were heated at 95°C for 5 min, and cell debris were removed after centrifugation. Protein concentrations were measured using the Bradford assay (Bio-Rad). 30 μg of proteins were separated by SDS-PAGE gels and transferred to polyvinylidene difluoride membranes

(PVDF, Bio-Rad) by electroblotting using a Trans-Blot Turbo blotting system (Bio-Rad). Custom made rabbit polyclonal antiphospho-RPS6 (P-RPS6) or anti-RPS6 (RPS6) antibodies were used (Dobrenel et al., 2016b). Membranes were blocked with a 5% non-fat dry milk solution in PBS (137 mM NaCl, 2.7 mM KCl, 10 mM $Na_2HPO_4$, 2 mM $KH_2PO_4$, pH7.4) and then probed overnight with either anti-P-RPS6 (dilution 1:2500) or with anti-RPS6 (dilution 1:5000) antibodies at 4°C. A goat anti-rabbit IgG-horseradish peroxidase (HRP) (Sigma-Aldrich, A0545) was used as a secondary antibody (dilution 1:5000). Immunodetection was performed by using enhanced chemiluminescent (ECL) substrates for HRP as recommended by the manufacturer (Clarity Western ECL blotting substrate Bio-Rad) and was visualized using a LAS-4000 system (Fujifilm). Transferred proteins on PVDF membranes were visualized by Coomassie staining to check for equal loading.

### Yeast Two-Hybrid Assays

The coding sequences of *LST8* (At3g18140), *RAPTOR* (At3g08850) and *AtYAK1* (At5g35980) genes were cloned in the two-hybrid vectors pGBKT7-GW / pGADT7-GW (Lu et al., 2010), using the Gateway technology (Invitrogen). The yeast strain PJ69-4A (James et al., 1996) was co-transformed according to Gietz et al. (1992) with two different plasmids: the pGBKT7-GW vector containing the GAL4 DNA binding domain (BD) fused to LST8 or RAPTOR and the pGADT7-GW vector containing the GAL4 DNA activation domain (AD) fused to AtYAK1. The transformants were selected on synthetic medium with dextrose (SD medium: 0.68% Yeast Nitrogen Base with ammonium sulfate (Sigma-Aldrich), 2% dextrose, 2% agar) supplemented with the required amino acids. To test the interaction colonies were grown overnight at 30°C in liquid SD medium supplemented with the required amino acids. Yeast cultures were diluted to an $OD_{600}$ of 1 and 10-fold serial dilutions were spotted onto SD selective agar plates. Interactions between BD and AD fusion proteins were scored by the relative yeast growth on SD media lacking His (-HIS) and containing 0.4 mM 3-amino-1, 2, 4 triazole.

### Bimolecular Fluorescence Complementation (BiFC) Assay in Nicotiana Benthamiana Leaves

The coding sequences of *LST8* (At3g18140), *RAPTOR* (At3g08850) and *AtYAK1* (At5g35980) genes were cloned in the pBiFP 1-4 vectors (Azimzadeh et al., 2008), using the Gateway technology (Invitrogen). Each gene was cloned in fusion to either the N-terminal (nYFP) or the C-terminal (cYFP) part of YFP, either as N- or C-terminal fusions and under the control of the 35S promoter. The different vectors were introduced in the *Agrobacterium tumefaciens* strain C58C1 (pMP90) by electroporation. The Agrobacterium cultures were grown overnight at 28°C until saturation, were collected by centrifugation and resuspended in infiltration buffer (10 mM $MgCl_2$, 10 mM MES pH 5.6). Equal volumes of Agrobacterium cultures expressing either cYFP or nYFP fusions were mixed and used for infiltration of abaxial leaf cells from *N. benthamiana* with a 1 mL syringe. Two days after infiltration YFP fluorescence in leaf epidermal cells was visualized by confocal microscopy Zeiss LSM 710.

### *In Vitro* Kinase Assay

For the TOR kinase assay, the coding sequence of *AtYAK1* was cloned into pDONR221, and the resulting entry vector was recombined with pDEST-His-MBP (Addgene 11085) for N-terminal fusion of the His-MBP tag and the recombinant protein was produced and purified as described by Van Leene et al. (2019). For *in vitro* kinase assays, the TOR kinase complex was purified by tandem affinity purification (TAP) from a PSB-D cell culture expressing the N-terminal $GS^{rhino}$ fusion to RAPTOR1B as previously described (Van Leene et al., 2019) and mixed with the recombinant His-MBP-AtYAK1 protein. After standard washing of streptavidin beads, the beads were washed with 250 μl kinase wash buffer (25 mM HEPES, pH 7.4, and 20 mM KCl). Washed beads were dissolved in 80 μl kinase assay buffer (25 mM HEPES, pH 7.4, 100mM NaCl, 50 mM KCl, 10 mM MgCl2 and 10 μM cold ATP). Kinase reactions were performed for 1 h at 30°C, combining 20 μl TAP-purified fractions with 10 μl substrate, in the presence of 5 μCi ATP-γ-$^{32}$P. As negative control, TAP purifications were performed on wild-type PSB-D cell cultures and streptavidin beads were combined with an equal amount of substrate. After the kinase reaction, the streptavidin beads were removed by centrifugation through Mobicol columns (MoBiTec GmbH, Germany) to remove the co-migrating RAPTOR band. Reactions were stopped by addition of SDS sample buffer and incubation for 10 min at 95°C. Proteins were separated by SDS–PAGE and stained with Coomassie Brilliant Blue R-250. Gels were dried and radioactivity was detected by autoradiography on a photographic film. YAK1 autophosphorylation was first inhibited by incubation with 25 μM INDY for 1hour at 30°C.

### Transcriptome Studies

Transcriptomes were analyzed using RNA-seq and RNA extracted from three independent biological replicates. Total RNA was extracted from 7-day-old seedlings using the RNeasy plant minikit (QIAGEN) including a DNase treatment according to manufacturer's instructions. Sequencing technology used an Illumina NexSeq500 (IPS2 POPS platform). RNA-seq libraries were performed by TruSeq Stranded protocol (Illumina®, California, U.S.A.). The RNA-seq samples have been sequenced in single-end (SE) with a sizing of 260 bp and a read length of 75 bases. 18 samples by lane of NextSeq500 using individual bar-coded adapters and giving approximately 16 millions of SE reads by sample are generated. All steps of the experiment, from growth conditions to bioinformatic analyses, were managed in CATdb database (Gagnot et al., 2008; http://tools.ips2.u-psud.fr/CATdb/) ProjectID NGS2018_05_TOR according to the international standard MINSEQE 'minimum information about a high-throughput sequencing experiment'.

### Metabolite Measurements

Metabolite levels were determined by global analysis after derivatization and injection into a GC-MS. *In vitro* grown seedlings were harvested 7 days after sowing on *Arabidopsis* medium. Four biological replicates were analyzed for each mutant and control lines. All extraction steps were performed in 2 mL Safelock Eppendorf tubes. The ground frozen samples (50 mg) were resuspended in 1 mL of frozen (−20°C) Water:Acetonitrile:Isopropanol (2:3:3) containing Ribitol at 4 μg/ml and extracted for 10 min at 4°C with shaking at 1400 rpm in an Eppendorf Thermomixer. Insoluble material was removed by centrifugation at 20000 g for 5 min. 50 μl were collected and dried overnight at 35°C in a Speed-Vac and stored at −80°C or immediately injected. Three Blank tubes underwent the same steps as the samples. A quality control was made by pooling an equal volume of each conditions. Samples were taken out of −80°C, warmed 15 min before opening and speed-vac dried again for 1.5 hour at 35°C before adding 10 μl of 20 mg/ml methoxyamine in pyridine to the samples and the reaction was performed for 90 min at 28°C under continuous shaking in an Eppendorf thermomixer. 90 μl of N-methyl-N-trimethylsilyl-trifluoroacetamide (MSTFA) (Aldrich 394866-10x1ml) were then added and the reaction continued for 30 min at 37°C. After cooling, 45 μl were transferred to an Agilent vial for injection. Four hours after derivatization 1 μl of sample was injected in splitless and split (1:30) modes on an Agilent 7890A gas chromatograph coupled to an Agilent 5977B mass spectrometer. The column was an Rxi-5SilMS from Restek (30 m with 10 m integraguard column). The liner (Restek # 20994) was changed before each series of 24 samples analysis. Oven temperature ramp was 70°C for 7 min then 10°C/min to 330°C for 5 min (run length 38 min). Helium constant flow was 0.7 mL/min. Temperatures were the following: injector: 250°C, transfer line: 290°C, source: 250°C and quadrupole 150°C. Five scans per second were acquired spanning a 50 to 600 Da range. The instrument was tuned with PFTBA with the 69 m/z and 219 m/z of equal intensities. Samples were randomized. Four different quality controls were injected at the beginning and end of the analysis for monitoring of the derivatization stability. An alkane mix (C10, C12, C15, C19, C22, C28, C32, C36) was injected in the middle of the queue for external RI calibration. Five scans per second were acquired. An injection in split mode with a ratio of 1:30 was systematically performed with the following conditions: 70°C for 2 min then 30°C per min to 330°C for 5 min. Helium constant flow 1 mL/min. Three independent derivatization of the quality control were injected at the beginning, in the middle and at the end of the series.

### Metabolic Data Processing

Raw Agilent datafiles were converted to NetCDF format and analyzed with AMDIS https://chemdata.nist.gov/mass-spc/amdis/. A home retention indices/mass spectra library built from the NIST, Golm, http://gmd.mpimp-golm.mpg.de/ and Fiehn databases and standard compounds was used for metabolite identification. Peak areas were also determined with the Targetlynx software (Waters) after conversion of the NetCDF file in masslynx format. AMDIS, Target Lynx in splitless and split 30 modes were compiled in one single Excel File for comparison. After blank mean substraction peak areas were normalized to Ribitol and Fresh Weight. Statistical analysis was made with TMEV http://mev.tm4.org/#/welcome: univariate analysis by permutation (1way-anova and 2-way anova) were first used to select the significant metabolites (P value < 0.01). Multivariate analysis (hierarchical clustering an principal component analysis) were then made on them. Mapman http://www.gabipd.org/projects/MapMan/ was used for graphical representation of the metabolic changes after $Log_2$ transformation of the mean of the 3 replicates (Thimm et al., 2004).

## QUANTIFICATION AND STATISTICAL ANALYSIS

### RNA-Seq Bioinformatic Treatment and Analysis

To facilitate comparisons, each sample followed the same steps from trimming to count. RNA-Seq preprocessing includes trimming library adapters and performing quality controls. The raw data (fastq) were trimmed with Trimmomatic (Bolger et al., 2014) tool for Phred Quality Score Qscore > 20, read length > 30 bases, and ribosome sequences were removed with tool sortMeRNA (Kopylova et al., 2012).

The mapper Bowtie version 2 (Langmead et al., 2009) was used to align reads against the *Arabidopsis thaliana* transcriptome (with–local option and other default parameters). The 33602 genes were extracted from TAIR10 database with one isoform per gene (corresponding to the longest CDS). The abundance of each gene was calculated by a local script which parses SAM files and counts only paired-end reads for which both reads map unambiguously one gene, removing multi-hits. According to these rules, around 98.4% of SE reads were associated to a gene, approximatively 2% SE reads unmapped and 1.85 to 2.2% of SE reads with multi-hits were removed.

Differential analysis followed the procedure described in Rigaill et al. (2018). Briefly, genes with less than 1 read after a count per million (CPM) normalization in at least one half of the samples were discarded. Library size was normalized using the trimmed mean of M-value (TMM) method and count distribution was modeled with a negative binomial generalized linear model where the environment factor (“stressed” or “unstressed” plants) and the block number were taken into account. Dispersion was estimated by the edgeR method (Version 1.12.0, McCarthy et al., 2012) in the statistical software ‘R’ (Version 2.15.0; R Development Core Team 2005). Expression differences were compared between stressed and unstressed plants using likelihood ratio test and p values were adjusted by the Benjamini-Hochberg procedure to control False Discovery Rate (FDR). A gene was declared differentially expressed if its adjusted p value < 0.05. FPKMs were calculated for visual analysis only, and were obtained by dividing normalized counts by

gene length. Expression differences were compared between the different mutants and Col0 WT using likelihood ratio test and pvalues were adjusted by the Benjamini-Hochberg procedure to control FDR. A gene was declared differentially expressed if its adjusted pvalue is lower than 0.05.

Gene ontology enrichment analysis was performed using the PlantGSEA online toolkit (http://structuralbiology.cau.edu.cn/PlantGSEA/index.php). Differentially expressed transcripts (adjusted $p < 0.05$; $\log_2$ fold change $> |0.5|$) were compared against the *Arabidopsis thaliana* genome, using Fisher's exact test and Yekutieli adjustment (FDR < 0.05) parameters.

### Metabolite Absolute Quantification

A response coefficient was determined for 4 ng each of a set of 103 metabolites, respectively to the same amount of ribitol. This factor was used to give an estimation of the absolute concentration of the metabolite in what we may call a ''one point calibration.''

### Growth Data Analysis

All statistical tests were done using XLSTAT. The non-parametric Kruskal-Wallis test was performed with pairwise multiple comparisons according to Conover-Iman tests and the addition of Bonferroni correction.

## DATA AND SOFTWARE AVAILABILITY

### RNA-Seq Data

RNA-Seq data were submitted to the GEO international repository (Gene Expression Omnibus, Edgar et al., 2002), https://www.ncbi.nlm.nih.gov/geo).

ProjetID: GEO: GSE120003.

### Metabolomic Data

Raw data are provided in Data S2.

**Cell Reports, Volume *27***

## Supplemental Information

# Mutations of the AtYAK1 Kinase Suppress TOR Deficiency in *Arabidopsis*

**Céline Forzani, Gustavo T. Duarte, Jelle Van Leene, Gilles Clément, Stéphanie Huguet, Christine Paysant-Le-Roux, Raphaël Mercier, Geert De Jaeger, Anne-Sophie Leprince, and Christian Meyer**

**Figure S1**

**A**

20 000 *lst8 1-1* seeds
mutagenized by 0.35% EMS

↓

1500 M1 plants
Screen 250 M2 pool of seeds
*In vitro*: Faster growing seedlings
In soil: Flower and set seeds faster

↓

**6 *sol* suppressor lines**
Back-cross M2 *sol* mutants
to *lst8-1-1*

↓

Identification of the mutations
by whole genome sequencing
of M2 plants

↓

Mutdetect pipeline
Identify homozygous mutations/lines

↓

*sol23*/*sol69*
stop/splice variant
in the At**YAK1** kinase (At5g35980)

↓

Confirm causal mutation in AtYAK1
by segregation analysis
and verification of SNP by CAPS

**B**

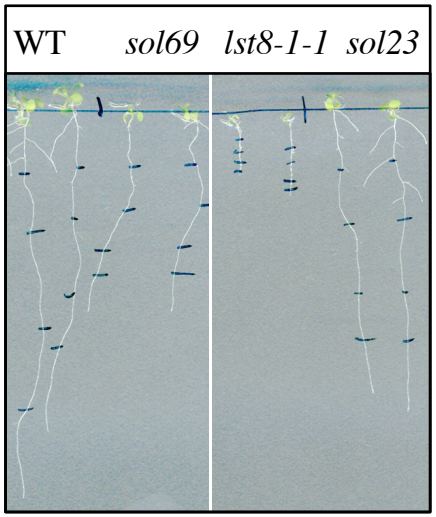


**C**

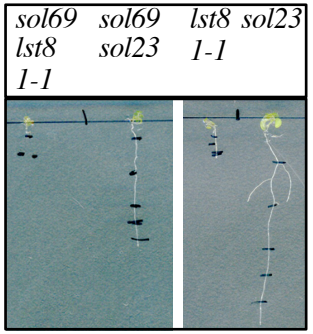


**D**

| Cross $F_2$ | non-supressed | suppressed |
|---|---|---|
| *sol23 lst8-1-1* | 83 | 23 |
| expected ratio | Chi-square $X^2$ | *P* value |
| 3:1 | 0.61 | 0.43 |

**E**

CAPS marker for AtYAK1

CATGTGGTCTTTTGG WT
CATGTGATCTTTTGG * mutation
*

MboI digest

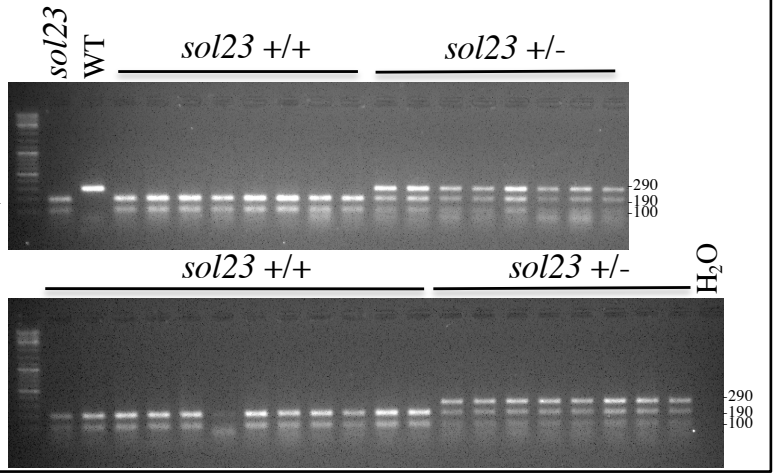

**Figure S1**. **Confirmation of the causal mutation in *sol23*. Related to Figure 1.** (A) Scheme showing the different steps of the *lst8-1-1* suppressor screen. (B) Root growth shown 12 days after transfer (DAT) on Arabidopsis medium. *Sol23* and *sol69* suppress the *lst8-1-1* root growth phenotype. (C) Allelism test. Seedlings of *lst8-1-1*, *sol23* and of the the F1 progeny from crosses between *lst8-1-1 sol69* and *sol69 sol23*. The seedlings were grown for 10 days after germination. The phenotype of the F1 cross between *sol69 sol23* was similar to *sol23* indicating that *sol23* and *sol69* are allelic with a mutation in the same gene. (D) *sol23* was backcrossed to *lst8-1-1* and the F2 population was further analysed. F2 plants were scored according to their phenotype: suppressed (plants in the blue box) and non-suppressed (plants in the yellow box). Chi-square analysis suggests that *sol23* behaves as a recessive mutation. (E) Diagram of the CAPS assay. Primers were designed using dCAPS Finder 2.0 to amplify a DNA fragment of AtYAK1 containing the SNP (in red). This new sequence is recognized by the restriction enzyme *Mbo*I. Therefore, the DNA fragment will be differentially cleaved by the restriction enzyme whether it is WT (uncleaved) or mutant (cleaved). Gel electrophoresis is then used to identify the size difference between WT and mutant PCR fragments. Homozygous *sol23* will be cleaved on both strands of the DNA (190 and 100 bp bands) and the WT (which is *lst8-1-1*) will not be cleaved (290 bp band). The F2 population described in (D) was further analyzed. (+) Represent the suppressed plants (blue box) and (–) the non-supressed plants (yellow box). Every plant showing the suppressed phenotype was homozygous for the *sol23* mutation and the non-suppressed plants were all heterozygous for *sol23*. The mutation in *AtYAK1* is very likely the causal mutation in *sol23* since it segregates with the suppressed phenotype.

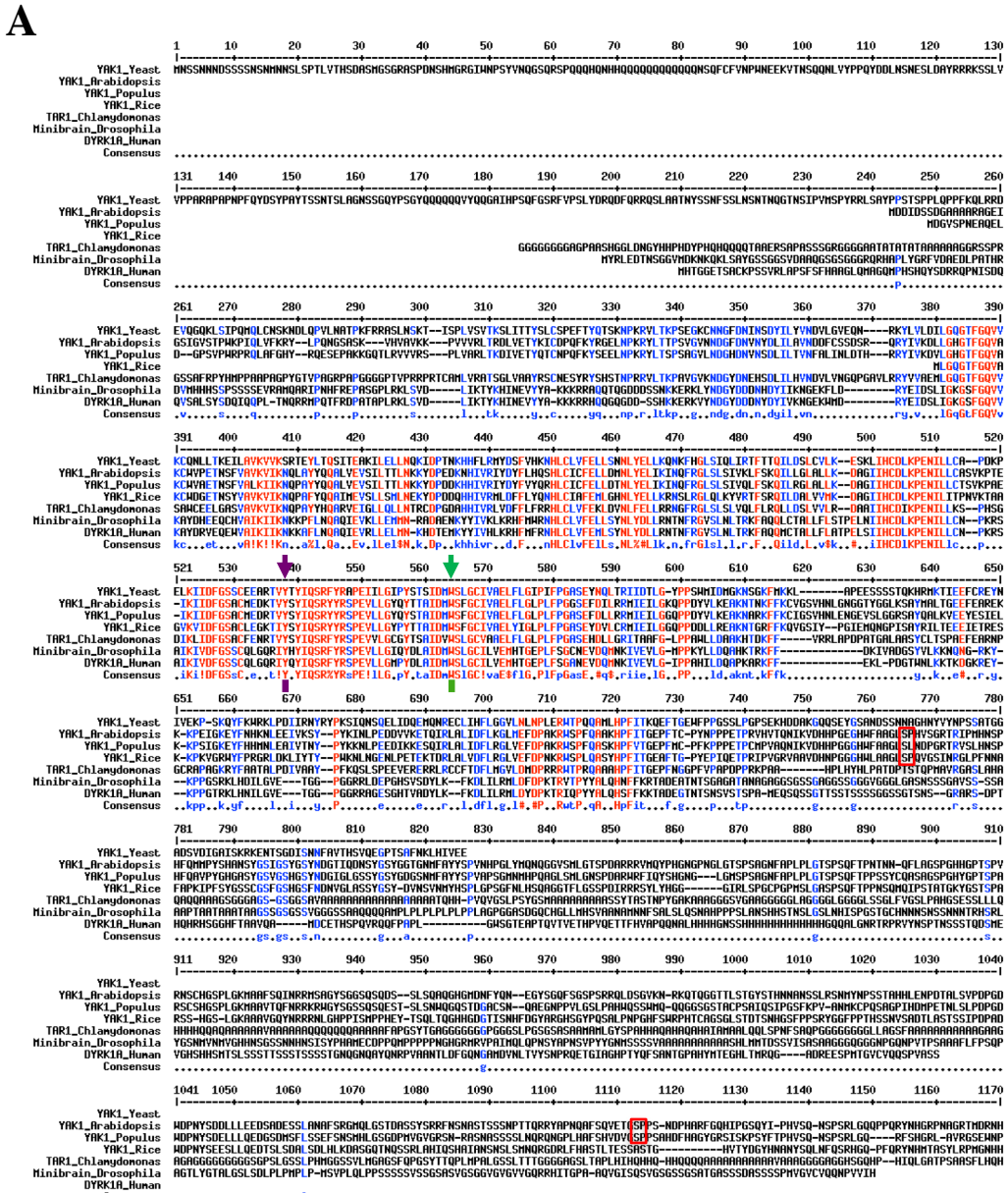


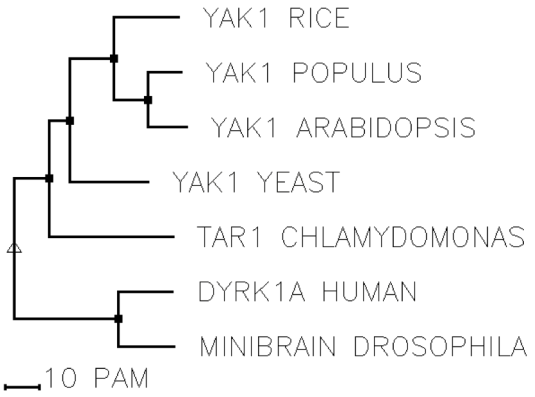


**Figure S2. Alignment of plants, yeast, Drosophila and human YAK1/DYRK protein sequences. Related to Figure 1.** (A) Multiple sequence alignment of YAK1/DYRK proteins. Conserved residues are shown in red. The W residue mutated in the *sol23* suppressor line is pointed by a green arrow. The activating Y residue is pointed by a purple arrow. Red boxes indicate putative TOR phosphorylation sites: Ser505 and Ser847 (Van Leene et al., 2019). The multiple alignment was performed using multalin (http://multalin.toulouse.inra.fr/). (B) Homology tree built from the aligned sequences.

**Figure S3**

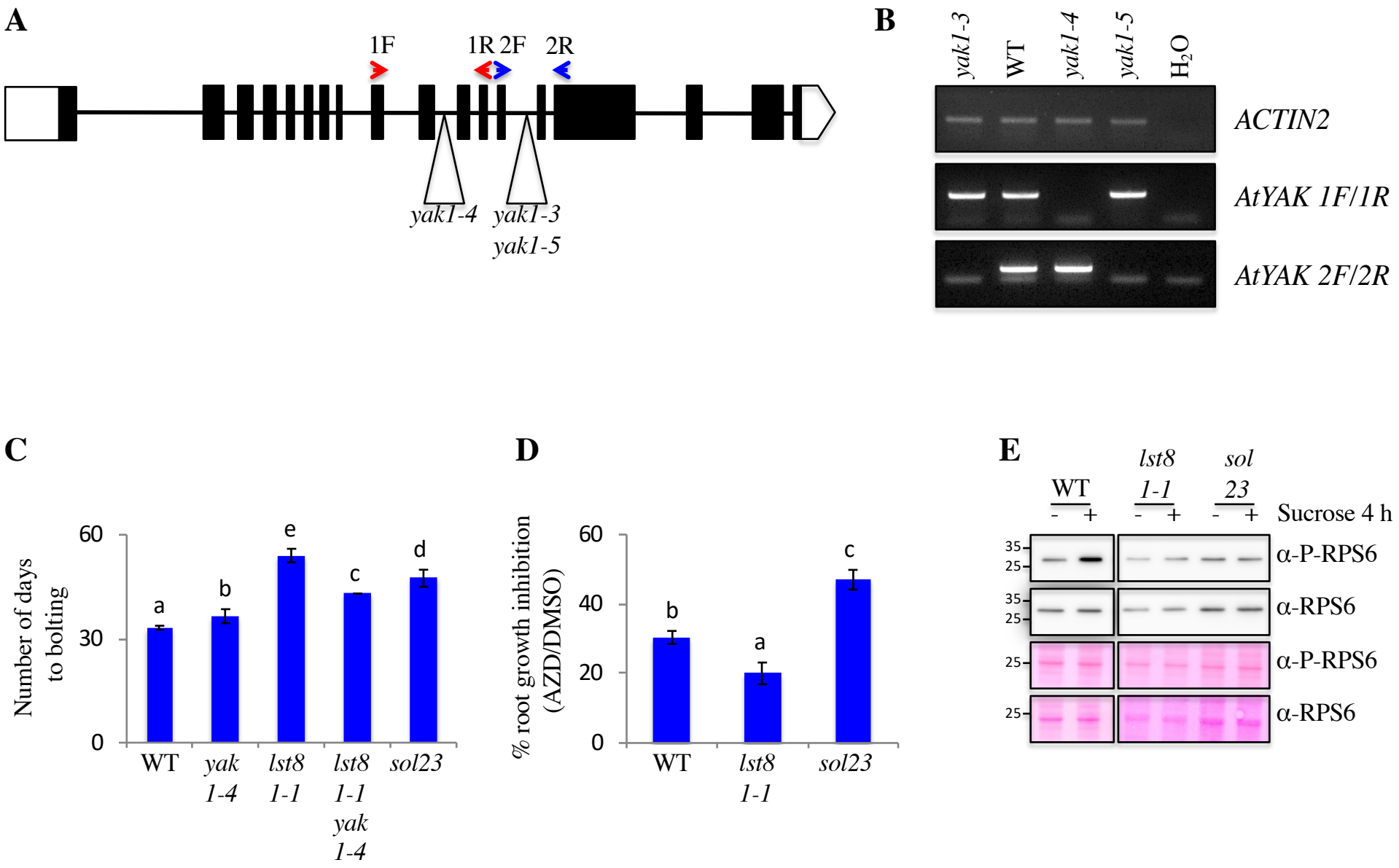
A
1F
1R 2F
2R
yak1-4
yak1-3
yak1-5
B
yak1-3
WT
yak1-4
yak1-5
H2O
ACTIN2
AtYAK 1F/1R
AtYAK 2F/2R
C
Number of days to bolting
60
30
0
a
b
e
c
d
WT
yak 1-4
lst8 1-1
lst8 1-1 yak 1-4
sol23
D
% root growth inhibition (AZD/DMSO)
60
40
20
0
b
a
c
WT
lst8 1-1
sol23
E
WT
lst8 1-1
sol 23
- +
- +
- +
Sucrose 4 h
35
25
α-P-RPS6
α-RPS6
α-P-RPS6
α-RPS6

**Figure S3**. **Absence of the *AtYAK1* transcript in the three *atyak1* mutant lines. Related to Figure 1, 2 and 3.**
(A) Schematic diagram of the *AtYAK1* gene showing the T-DNA insertions site (represented by triangles) of the different *atyak1* mutants used in the study as well as the primers used for the RT-PCR analysis. (B) RT-PCR analysis showing the levels of *AtYAK1* transcripts in the various homozygous *atyak1* mutants. The *ACTIN2* gene was used as an internal standard. By using primers spanning each side of the T-DNA, each *atyak1* allele showed absence of the corresponding *AtYAK1* transcript. ***sol23* rescues *lst8-1-1* growth defects and shows altered TOR signaling.** (C) Quantification of the flowering time by measuring the number of days to bolting. Plants were grown in LD conditions. Twelve plants were measured for each genotype. Two independent experiments were performed with similar results. Identical WT, *yak1-4*, *lst8-1-1* and *lst8-1-1 yak1-4* are shown in Figure 2. Error bars indicate the standard deviation of a single experiment. Letters indicate significantly different classes (non-parametric Kruskal-Wallis test, $p < 0.05$). (D) Quantification of the root length 7 DAT on Arabidopsis medium supplemented with 0.5 or 1 $\mu$M AZD-8055. Between 10 to 20 seedlings were measured for each genotype with three biological replicates. Error bars indicate the standard deviation of three independent experiments. Letters indicate significantly different classes (non-parametric Kruskal-Wallis test, $p < 0.05$). (E) Determination of TOR activity using phosphorylation of the ribosomal protein S6 as a readout. Total protein extracts from seedlings were used for immunoblotting with a phospho-specific antibody against phosphorylated RPS6 ($\alpha$-P-RPS6) or an antibody recognizing total RPS6 ($\alpha$-RPS6). Bottom panels show the Coomassie staining of the membrane. Six-day-old seedlings from WT, *lst8-1-1* and *sol23* were transferred to sugar-free medium for 24 h and then either mock (-) or 0.5 % sucrose (+) treated for 4 h.

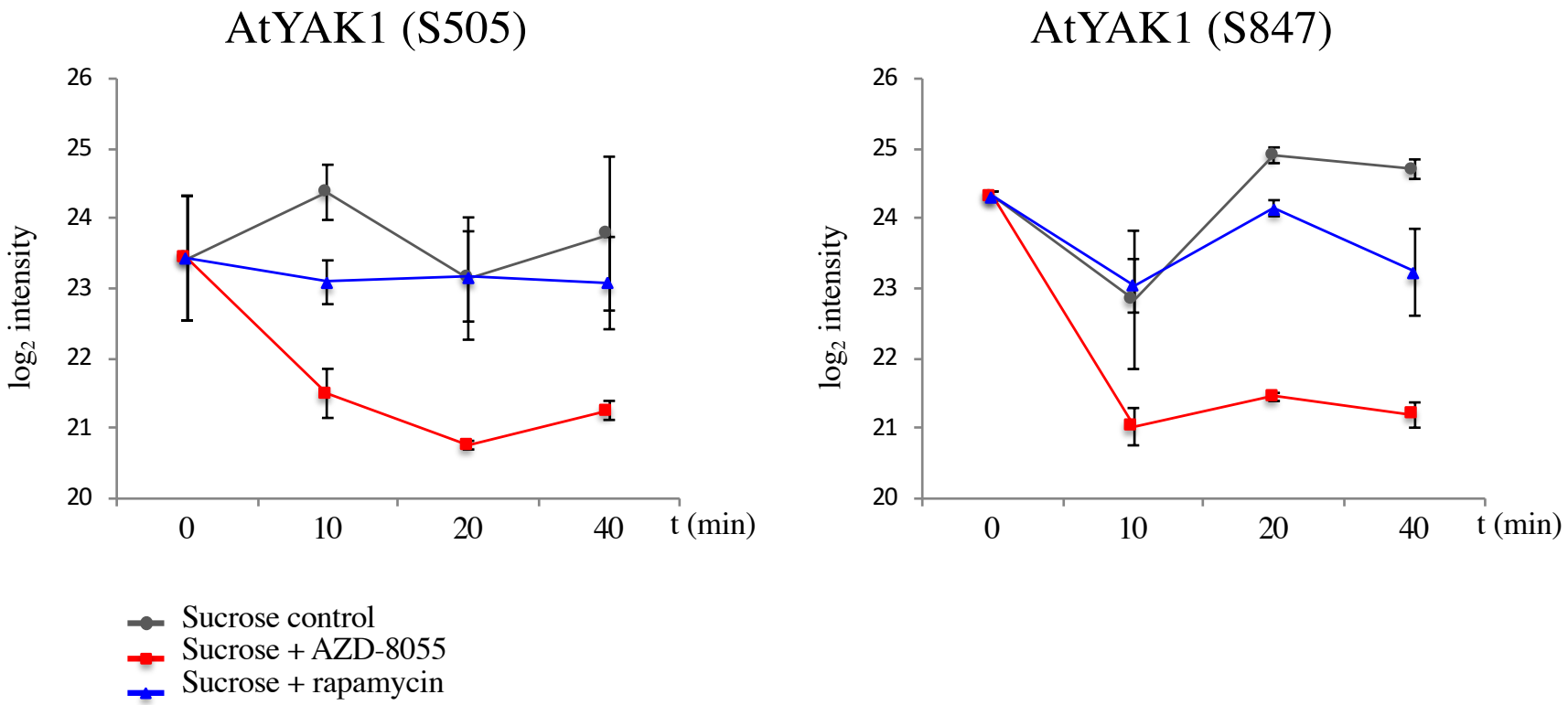


**Figure S4. Phosphopeptide intensity plots for the AtYAK1 protein. Related to Figure 4.**

Phosphopeptides are quantified at different time points after sucrose addition, AZD-8055 or rapamycin treatment of cell cultures. Ser505 and Ser847 are putative TOR phosphorylation sites found in the AtYAK1 protein. AtYAK1 phosphorylation is inhibited after the addition of the TOR inhibitor AZD-8055. Error bars indicated the standard error of four independent experiments. Data were extracted from Van Leene et al. (2019) in which experimental details can be found.

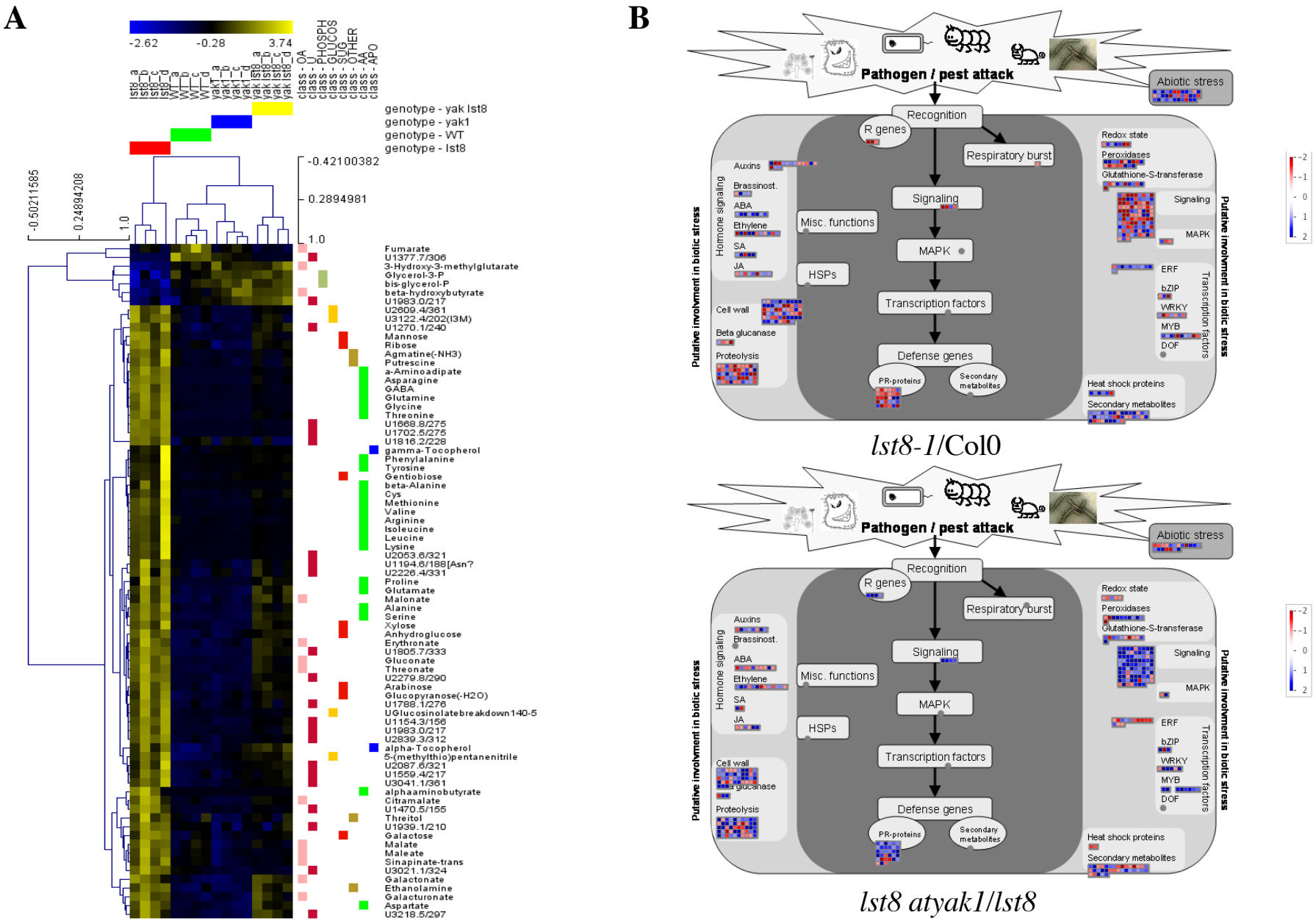


**Figure S5**. **Global metabolite profiling with GC-MS. Related to Figure 5.** (A) Hierarchical clustering analysis (HCA) of metabolites of four different genotypes: *lst8* = *lst8-1-1*, WT = Col-0, *yak1* = *atyak1-4*, *yak lst8* = *lst8-1-1 atyak1-4*. Approximately 200 seedlings were used for each genotype with four biological repeats (a-d). The intensity of the blue and yellow colours indicates low or high amount of metabolites respectively with the scale positioned above the HCA. (B) Mapman representation of differentially expressed gene families regulated in the *lst8-1-1* and *lst8-1-1 atyak1* mutants. See Star Methods for details.

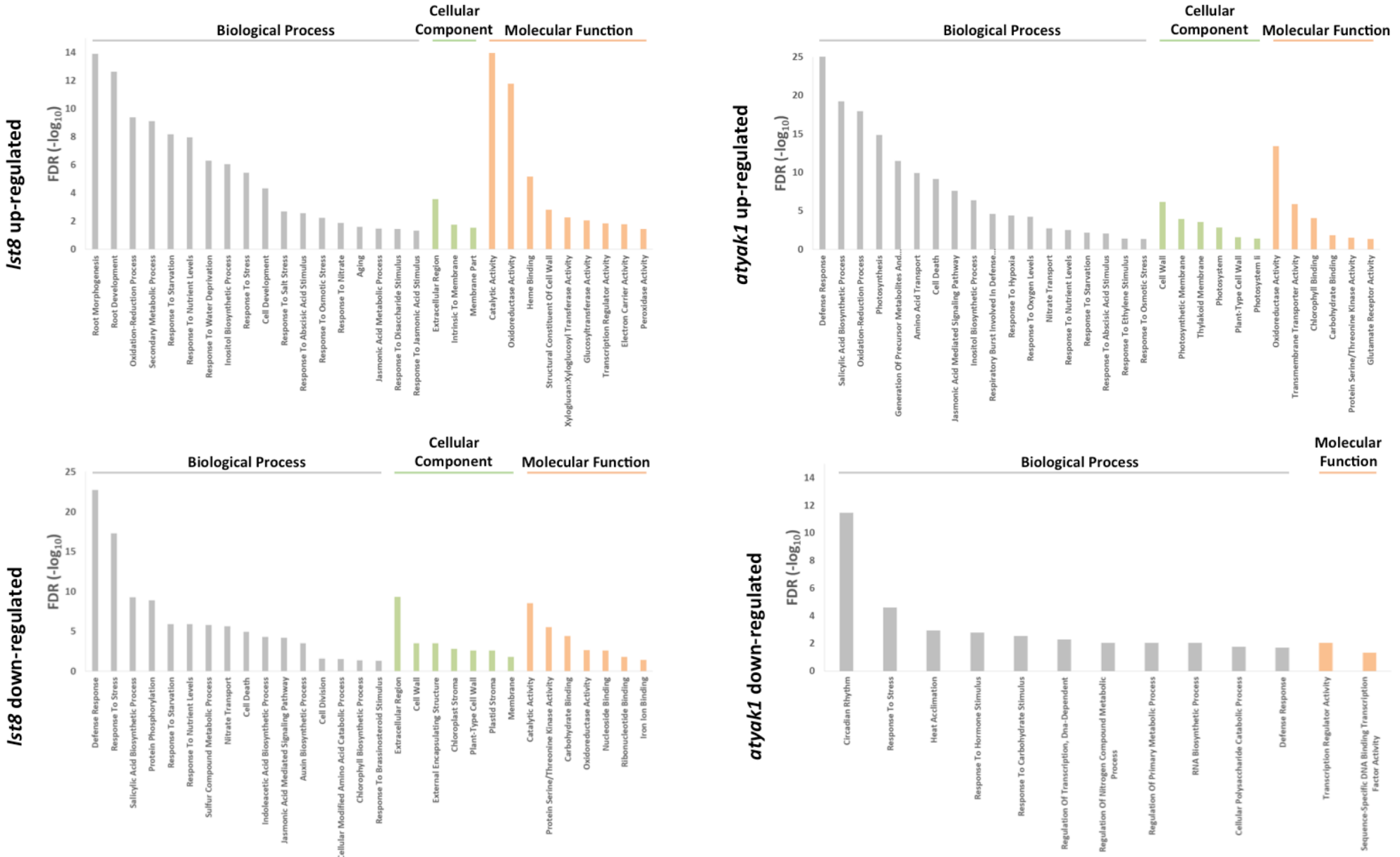


**Figure S6. Enrichment in functional classes of differentially regulated genes in the transcriptomic analysis. Related to Figure 6.**
Selected gene ontology enriched terms (FDR < 0.05) of *lst8* (*lst8-1-1)* and *atyak1* (*atyak1-4)* up- or down-regulated transcripts (adjusted $p < 0.05$ and $\log_2$ fold change >|0.5| in comparison to the wild type). The statistical enrichment significance is represented on the y-axis as the $-\log_{10}$ value of the FDR.

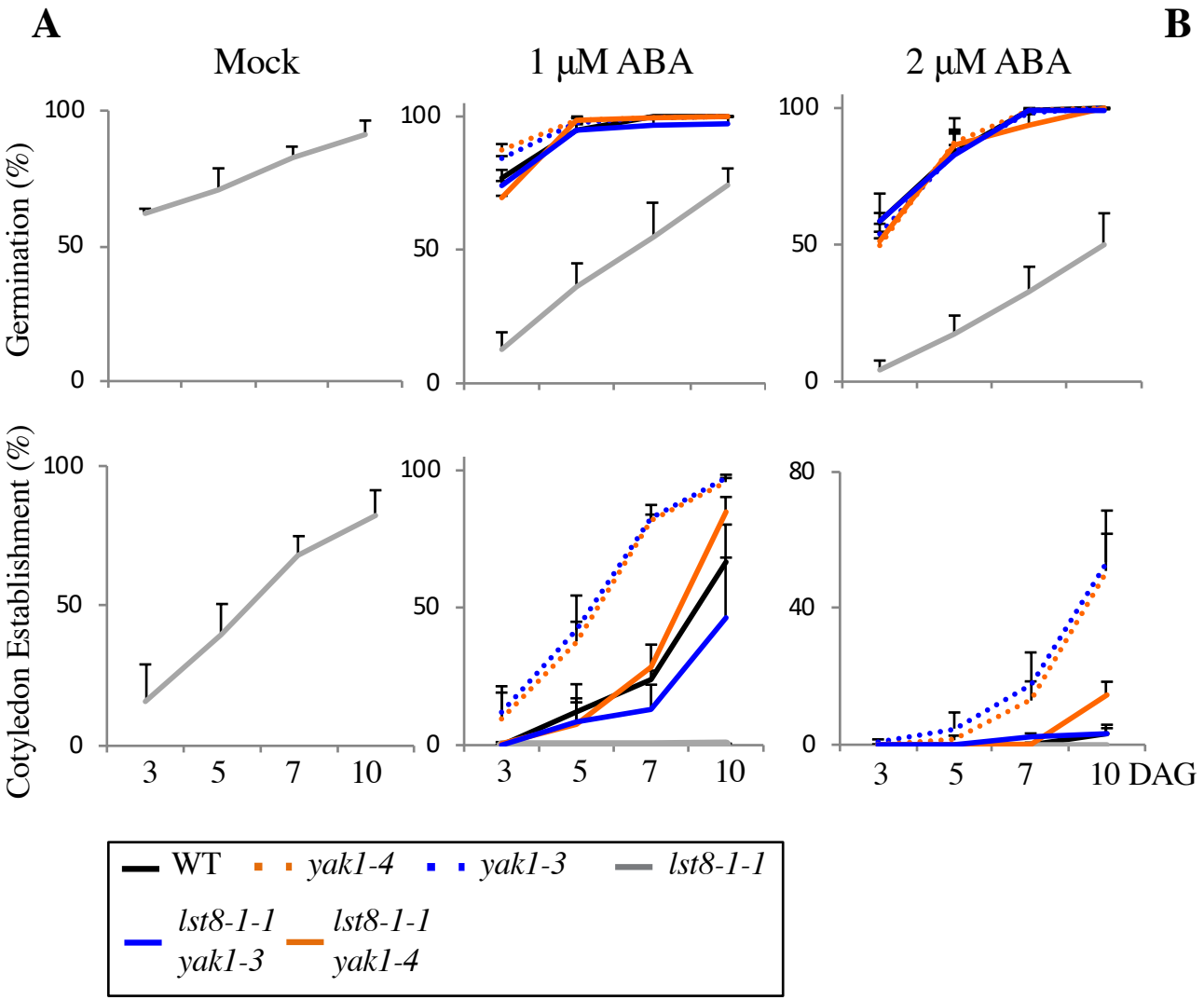


B

N metabolism

| | | lst8-1 /Col | lst8yak1 /lst8 |
|---|---|---|---|
| AT2G24720 | ATGLR2.2 (Arabidopsis thaliana glutamate receptor 2.2) | -3,03 | 2,72 |
| AT2G24710 | ATGLR2.3 (Arabidopsis thaliana glutamate receptor 2.3) | -2,79 | 1,63 |
| AT1G08090 | ATNRT2:1 (Arabidopsis thaliana high affinity nitrate transporter 2.1); nitrate transporter | -1,89 | 1,38 |
| AT4G31710 | ATGLR2.4 (Arabidopsis thaliana glutamate receptor 2.4) | -1,83 | 1,73 |
| AT3G45060 | ATNRT2.6 (Arabidopsis thaliana high affinity nitrate transporter 2.6); nitrate transporter | -1,70 | 0,83 |
| AT5G27100 | ATGLR2.1 (Arabidopsis thaliana glutamate receptor 2.1) | -1,49 | 1,53 |
| AT5G60780 | ATNRT2.3 (Arabidopsis thaliana high affinity nitrate transporter 2.3); nitrate transporter | -1,35 | 0,41 |
| AT2G29110 | ATGLR2.8 (Arabidopsis thaliana glutamate receptor 2.8) | -1,34 | |
| AT3G24300 | ATAMT1;3 (ammonium transporter 1;3); ammonium transporter | -1,27 | 0,99 |
| AT1G77760 | NIA1 (NITRATE REDUCTASE 1) | -1,07 | 0,71 |
| AT5G16570 | GLN1;4 (Glutamine synthetase 1;4); glutamate-ammonia ligase | -0,89 | |
| AT2G32390 | ATGLR3.5 (GLUTAMATE RECEPTOR 6) | -0,70 | |
| AT2G38290 | ATAMT2 (AMMONIUM TRANSPORTER 2) | -0,65 | 0,83 |
| AT2G29120 | ATGLR2.7 (Arabidopsis thaliana glutamate receptor 2.7) | -0,61 | 1,50 |
| AT1G66200 | ATGSR2 (Arabidopsis thaliana glutamine synthase clone R2); glutamate-ammonia ligase | -0,60 | 0,63 |
| AT1G64780 | ATAMT1;2 (AMMONIUM TRANSPORTER 1;2); ammonium transporter | -0,55 | 0,37 |
| AT1G78680 | ATGGH2 (GAMMA-GLUTAMYL HYDROLASE 2); gamma-glutamyl hydrolase | -0,35 | 0,33 |
| AT2G15620 | NIR1 (NITRITE REDUCTASE); ferredoxin-nitrate reductase | -0,30 | 0,41 |
| AT5G37600 | ATGSR1 (Arabidopsis thaliana glutamine synthase clone R1); glutamate-ammonia ligase | -0,30 | |
| AT1G12110 | NRT1.1 (nitrate transporter 1.1); transporter | | 0,26 |
| AT2G31955 | CNX2 (COFACTOR OF NITRATE REDUCTASE AND XANTHINE DEHYDROGENASE 2) | | 0,30 |
| AT2G02040 | ATPTR2-B (NITRATE TRANSPORTER 1); transporter | | 0,57 |
| AT4G01900 | GLB1 (glutamine synthetase B1) | | -0,24 |
| AT5G35630 | GS2 (GLUTAMINE SYNTHETASE 2) | | 0,69 |
| AT1G69850 | ATNRT1:2 (NITRATE TRANSPORTER 1:2); calcium ion binding / transporter | | -0,27 |
| AT5G04140 | GLU1 (FERREDOXIN-DEPENDENT GLUTAMATE SYNTHASE 1) | | 0,51 |
| AT1G78660 | ATGGH1; gamma-glutamyl hydrolase | 0,27 | |
| AT5G48400 | ATGLR1.2 (Arabidopsis thaliana glutamate receptor 1.2) | | 1,67 |
| AT3G53260 | PAL2 (phenylalanine ammonia-lyase 2); phenylalanine ammonia-lyase | 0,38 | -0,19 |
| AT5G65720 | ATNIFS1/NIFS1 (ARABIOPSIS THALIANA NITROGEN FIXATION S HOMOLOG 1) | 0,41 | -0,32 |
| AT1G58290 | HEMA1; glutamyl-tRNA reductase | 0,43 | 0,30 |
| AT3G10050 | OMR1 (L-O-METHYLTHREONINE RESISTANT 1); threonine ammonia-lyase | 0,44 | -0,24 |
| AT3G10340 | phenylalanine ammonia-lyase, putative | 0,48 | -0,23 |
| AT5G17330 | GAD (Glutamate decarboxylase 1); calmodulin binding | 0,50 | |
| AT1G37130 | NIA2 (NITRATE REDUCTASE 2) | 0,51 | 0,29 |
| AT2G37040 | PAL1 (PHE AMMONIA LYASE 1); phenylalanine ammonia-lyase | 0,52 | |
| AT3G17820 | ATGSKB6 (Arabidopsis thaliana glutamine synthase clone KB6); glutamate-ammonia ligase | 0,62 | -0,44 |
| AT1G63660 | GMP synthase (glutamine-hydrolyzing), putative / glutamine amidotransferase, putative | 0,65 | -1,00 |
| AT5G11210 | ATGLR2.5 (Arabidopsis thaliana glutamate receptor 2.5) | 0,96 | 0,76 |
| AT4G31730 | GDU1 (GLUTAMINE DUMPER 1) | 1,06 | -0,83 |
| AT5G56860 | GNC (GATA, NITRATE-INDUCIBLE, CARBON METABOLISM-INVOLVED); transcription factor | 1,18 | -0,29 |
| AT5G63270 | nitrate-responsive NOI protein, putative | 1,20 | -1,13 |
| AT3G21670 | nitrate transporter (NTP3) | 1,35 | 0,34 |
| AT5G07440 | GDH2 (GLUTAMATE DEHYDROGENASE 2); oxidoreductase | 1,77 | -1,24 |

**Figure S7. ABA and nitrogen responses. Related to Figure 7.**

(A) *AtYAK1* mutations suppress the ABA hypersensitivity of *lst8-1-1* mutants. Quantification of germination and of cotyledon establishment on media supplemented with DMSO (mock control), 1 or 2 $\mu$M ABA. Three days after germination, except for *lst8-1-1* all the other genotypes showed between 95 % and 100 % germination or cotyledon establishment. Between 45 to 80 seeds were used for each genotype. Error bars indicate the standard error of three independent experiments. DAG: Days after germination. (B) Transcriptomic analysis of genes differentially regulated in the *lst8-1-1* and *lst8-1-1 atyak1* mutants. A selection of nitrogen-related genes showing differential expression in the *lst8-1-1* mutant and the *lst8-1-1 atyak1* double mutant.

| | |
|---|---|
| CAPS-For | TTTGGCCAACTTGCGTTAACT |
| CAPS-Rev | ATACCCTAGTATTTCAATCATACGC |
| Actin-For | GCCATCCAAGCTGTTCTCTC |
| Actin-Rev | CCCTCGTAGATTGGCACAGT |
| Yak-1F | CACTATTTCCAGGAGGTTCAGA |
| Yak-1R | TGACCAACGTTTTGCTGGAT |
| Yak-2F | GCAAAGCACCCTTTCATTACT |
| Yak-2R | ATTGCCAGTCCCTCCATAGC |
| LBsail | TAGCATCTGAATTTCATAACCAATCTCGATACAC |
| LB1-3 | ATTTTGCCGATTTCGGAAC |

Primers used for genotyping
*yak1-4:* 1F+1R
*yak1-3:* 2F+2R
*yak1-5:* 2F+2R

**Table S1. List of primers. Related to Star Methods.** Oligonucleotides sequences are listed in the 5' -> 3' orientation.